Overexpression of the SETD2 WW domain inhibits the phosphor-IWS1/SETD2 interaction and the oncogenic AKT/IWS1 RNA splicing program.

Georgios I. Laliotis[1,2,3,8*], Evangelia Chavdoula[1,2], Vollter Anastas[1,2,4], Satishkumar Singh[5], Adam D. Kenney[6,7], Samir Achaya[1,2,9], Jacob S. Yount[6,7], Lalit Sehgal[2,5] and Philip N. Tsichlis[1,2,*]

[1]The Ohio State University, Department of Cancer Biology and Genetics, Columbus, OH, 43210, [2]The Ohio State University Comprehensive Cancer Center-Arthur G. James Cancer Hospital and Richard J. Solove Research Institute, Columbus, OH, 43210, [3]University of Crete, School of Medicine, Heraklion Crete, 71500, Greece, [4]Tufts Graduate School of Biomedical Sciences, Program in Genetics, Boston, MA, 02111, USA, [5]College of Medicine, Department of Hematology, The Ohio State University, Columbus, OH 43210, [7]Department of Microbial Infection and Immunity, The Ohio State University, Columbus, OH, 43210

Running Title: SETD2 WW domain inhibits the IWS1 RNA splicing program

Present address :

[8]Department of Oncology, Sidney Kimmel Comprehensive Cancer Center, Johns Hopkins School of Medicine, Baltimore, MD, 21231

[9]Nationswide Children's Hospital, Columbus, OH, 43205

*Correspondence should be addressed to: Philip N. Tsichlis (Lead contact) (Philip.tsichlis@osumc.edu) and Georgios I. Laliotis (glaliot1@jhmi.edu)

Abstract

Our earlier studies had shown that AKT phosphorylates IWS1, and that following phosphorylation, IWS1 recruits the histone methyltransferase SETD2 to an SPT6/IWS1/ALY complex, which assembles on the Ser2-phosphorylated CTD of RNA Pol II. Recruited SETD2 methylates histone H3 at K36, during transcriptional elongation of target genes, and this regulates multiple steps in RNA metabolism. By regulating the RNA splicing of *U2AF2,* it controls cell proliferation. Importantly, pathway activity correlates with grade, stage and metastatic potential of lung adenocarcinomas, especially those with *EGFR* mutations. By regulating nucleocytoplasmic mRNA transport of intronless genes, including those encoding type I IFNs, it regulates sensitivity to viral infection. Here, we show that SETD2 interacts with IWS1 via its WW domain, that the interaction is IWS1 phosphorylation-dependent and that WW domain overexpression blocks the interaction and inhibits the pathway and its biological outcomes. We conclude that blocking the phosphor-IWS1/SETD2 interaction is feasible and has significant therapeutic potential in human cancer.

59 **Introduction**

60 Earlier studies had shown that IWS1 interacts with, and recruits SETD2 to an
61 SPT6/IWS1/ALY complex, which assembles on the Ser2-phosphorylated CTD of RNA Pol II
62 (Yoh et al., 2007[1]) and that the SETD2 recruitment depends on the phosphorylation of IWS1
63 at Ser720/Thr721 by AKT (Sanidas et al., 2014[2], Laliotis et al., 2021[3]). The binding of SETD2
64 to the SPT6/phospho-IWS1 complex results in trimethylation of histone H3 at K36 during
65 transcriptional elongation. Whereas the phosphorylation of IWS1 regulates the recruitment of
66 SETD2, it does not affect the interaction between IWS1 and the other components of the
67 SPT6/IWS1/ALY/SETD2 complex.

68 The recruitment of SETD2 to the SPT6/IWS1/ALY complex and the trimethylation of
69 histone H3 in the body of genes targeted by this complex, has profound effects on the biology
70 of NCI-H522 and other NSCLC cell lines. Our earlier studies had shown that it regulates the
71 alternative RNA splicing of *FGFR2*, favoring the *FGFR2* IIIc splice variant (Sanidas et al.,
72 2014[2]), which is primarily expressed in mesenchymal cells (Luco et al., 2010[4]), and which, in
73 cancer cells, promotes epithelial to mesenchymal transition and cell migration, invasiveness
74 and metastasis (Thiery et al., 2006[5]). RNA-Seq studies, comparing the gene expression
75 profiles of NCI-H522 cells transduced with shControl, or shIWS1 constructs, and shIWS1-
76 transduced NCI-H522 cells rescued with wild type IWS1 (WT-R) or with the phosphorylation
77 site IWS1 mutant (MT-R), revealed genome wide IWS1 and IWS1 phosphorylation-dependent
78 changes in gene expression and RNA processing (Laliotis et al., 2021[3]). Importantly, many of
79 the genes whose expression and/or RNA processing were deregulated in shIWS1 and
80 shIWS1/MT-R cells, were genes encoding proteins involved in epigenetic regulation and RNA
81 processing.

82 One of the genes undergoing IWS1 phosphorylation-dependent alternative RNA
83 splicing, is the *U2AF2* gene, which encodes the core RNA splicing factor U2AF65. The
84 predominant *U2AF2* mRNA in empty vector (shControl) and shIWS1/WT-R cells contain exon
85 2, which is absent from the predominant *U2AF2* mRNA in shIWS1 and shIWS1/MT-R cells.
86 Exon 2 encodes part of the N-terminal RS domain of U2AF65, which interacts with several

87 proteins involved in the regulation of RNA processing. One of these proteins is Prp19, a
88 member of an RNA splicing complex with ubiquitin ligase activity (Prp19C), which is composed
89 of four core and three accessory polypeptides and plays a critical role in spliceosomal
90 activation (Chanarat et al., 2013[6]). Prp19 is recruited to the phosphorylated CTD of RNA Pol
91 II, via its interaction with U2AF65. In vitro RNA splicing experiments have shown that the
92 U2AF65/Prp19 binding promotes the splicing of exons located downstream of weak
93 polypyrimidine tracts (David et al., 2011[7]). Our more recent studies provided evidence that by
94 regulating *U2AF2* RNA splicing, IWS1 phosphorylation promotes the expression of *CDCA5*,
95 which encodes Sororin, a member of the Cohesin complex, and that by regulating this
96 pathway, IWS1 phosphorylation plays a critical role in cell cycle regulation and cell proliferation
97 (Laliotis et al., 2021[3]). In addition, IWS1 phosphorylation-dependent RNA splicing promotes
98 the nucleocytoplasmic transport of the mRNAs of intronless genes that harbor Cytoplasmic
99 Accumulation Region Elements (CAR-E). This set of genes includes the genes encoding type
100 I interferons, whose expression is impaired when the pathway is disrupted (Laliotis et al.,
101 2021[8]). Most important, the IWS1 phosphorylation pathway correlates positively with the
102 grade, stage and metastatic potential of lung adenocarcinomas, especially those with
103 activating mutations or amplification of the gene encoding EGFR. As a result, patients with
104 EGFR mutant lung adenocarcinomas exhibit higher relapse rates after treatment, and
105 shortened survival (Laliotis et al., 2021[3]).

106 Based on the preceding observations, we hypothesized that targeting this pathway
107 may have significant therapeutic implications in lung adenocarcinomas with EGFR mutations,
108 and perhaps in other types of human cancer. Inhibiting AKT3, the AKT isoform primarily
109 responsible for the activation of the pathway, should block this pathway. However, we do not
110 currently have clinical grade AKT3 specific inhibitors and even if we did, inhibition of AKT3
111 would have multiple off target effects, because AKT3 does not only regulate this pathway.
112 Based on these considerations, we proceeded to investigate whether inhibiting the interaction
113 between IWS1 and SETD2 is feasible, and what would be the biological consequences of
114 blocking this interaction. The IWS1 domain interacting with SETD2 had been mapped earlier

115 to a sequence which extends from amino acid 522 to amino acid 698 and includes part of the
116 TFIID homologous IWS1 domain (Yoh et al., 2008[9]). As a first step therefore, we mapped the
117 SETD2 domain interacting with phosphorylated IWS1, and we showed that it is limited to a 40
118 amino acid peptide, which includes the 30 amino acid WW domain of SETD2. Following
119 mapping of the interacting domains, we showed that the WW domain of SETD2 interacts
120 preferentially with the phosphorylated form of IWS1, and that when overexpressed, it block
121 the interaction of the two proteins and inhibits the pathway activated via this interaction. More
122 important, overexpression of the WW domain of SETD2, inhibits tumor cell proliferation in
123 culture and tumor growth in xenograft models in animals, suggesting that blocking the
124 interaction of SETD2 with phosphorylated IWS1 is feasible and has significant therapeutic
125 potential in human cancer.

126 **Results**

127 **The interaction between SETD2 and phosphorylated IWS1 is mediated by the WW**
128 **domain of SETD2.**

129 Our first task prior to developing strategies to block the AKT phosphorylation-dependent
130 interaction between IWS1 and SETD2, was to map the SETD2 domain interacting with
131 phosphorylated IWS1. To this end, we generated a series of Hemagglutinin (HA)-tagged
132 deletion mutants of SETD2 (**Fig. 1a**), which we expressed via transient transfection in the NCI-
133 H522 and NCI-H1299 lung adenocarcinoma cell lines and we used co-immunoprecipitation to
134 determine their interaction with endogenous IWS1. Based on these experiments we mapped
135 the IWS1-interacting SETD2 domain to a 40 amino acid peptide, which includes the 33 amino
136 acid WW domain (aa 2388-2422) and surrounding sequences (**Fig. 1b and 1c**).

137 **The WW domain of SETD2 binds selectively IWS1 phosphorylated at Ser720/Thr721 and**
138 **disrupts the interaction of IWS1 with SETD2**

139 Our earlier studies had shown that SETD2 is recruited to an SPT6/IWS1/ALY-REF
140 complex, following phosphorylation of IWS1 at Ser720/Thr721, by AKT1 or AKT3. This
141 observation raised the question whether the binding of the WW peptide of SETD2 to IWS1
142 also depends on IWS1 phosphorylation. To address this question, we expressed Flag-tagged
143 constructs of wild type IWS1 or its phosphorylation site mutant in the lung adenocarcinoma
144 cell lines NCI-H522, NCI-H1299, A549 and NCI-H1975. Following this, we transduced the
145 cells with a V5-tagged construct of the SETD2 WW domain. Probing V5 (WW domain)
146 immunoprecipitates with the Flag-tag (IWS1) antibody and Flag-tag immunoprecipitates with
147 the V5 tag antibody, revealed that the WW domain of SETD2 indeed interacts with IWS1, but
148 the interaction is significantly more robust with wild type than with mutant IWS1 (**Fig. 2a**).
149 These observations strongly suggest that the interaction of the WW domain of SETD2 with
150 IWS1 continues to be IWS1 phosphorylation-dependent and therefore physiologically
151 relevant.

152 Following the demonstration that the WW domain of SETD2 interacts selectively with
153 phosphorylated IWS1, we examined whether overexpression of this domain inhibits the
154 IWS1/SETD2 interaction. First, we addressed the interaction of exogenous Flag-tagged wild
155 type IWS1, or IWS1-S720A/T721A with HA-SETD2, and following this, the interaction of the
156 endogenous proteins. Co-immunoprecipitation experiments confirmed that the overexpression
157 of the WW domain of SETD2 inhibits the interaction of both the exogenous and the
158 endogenous proteins (**Fig. 2b and 2c**).

159 **Overexpression of the SETD2 WW domain inhibits the IWS1 phosphorylation-**
160 **dependent RNA splicing program.**

161 The observation that overexpression of the SETD2 WW domain blocks the interaction
162 between phosphorylated IWS1 and SETD2, suggested that it would also interfere with IWS1

163 phosphorylation-dependent alternative RNA splicing. Our earlier studies identified several
164 IWS1 phosphorylation-dependent RNA splicing targets, including *U2AF2* (exon 2), *SLC12A2*
165 (exon 21), *IFT88* (exon 8), *C1qTNF6* (exon 3), *STXBP1* (exon 18) and *FGFR2* (exon 8)
166 (Laliotis et al., 2021[3] , Sanidas et al., 2014[2]). Transduction of the four lung adenocarcinoma
167 cell lines used for the experiments in figure 2 with a pLx304-based lentiviral construct of the
168 SETD2 WW domain revealed that overexpression of this domain reproduces the alternative
169 RNA splicing pattern of the IWS1 knockdown in all six genes (**Fig. 3a, 3d**). To determine
170 whether the WW domain-induced changes in alternative RNA splicing are due to inhibition of
171 the IWS1 phosphorylation pathway, we examined the binding of SETD2 and the abundance
172 of H3K36me3 marks, in selected regions of the *U2AF2* and *FGFR2* genes in NCI-H522 and
173 NCI-H1299 cells transduced with the pLx304-WW domain construct. The *U2AF2* and *FGFR2*
174 Transcription Start Sites (TSS) and *GAPDH* Exon 3 (E3) were used as controls. This was
175 addressed with chromatin Immuno Cleavage (ChIC) experiments, which showed that the WW
176 domain of SETD2 dramatically inhibits the binding of SETD2 and the abundance of histone
177 H3K36me3 marks (**Fig. 3c, 3d**). These experiments provided proof of principle for the
178 feasibility of blocking the IWS1/SETD2 interaction and for the ability of the block to inhibit the
179 IWS1 phosphorylation-dependent regulation of RNA processing. Based on our earlier findings
180 on the biology elicited by the IWS1 phosphorylation pathway, these data also suggested the
181 blocking this pathway by overexpressing the SETD2 WW peptide should have a major impact
182 on the pathobiology of lung adenocarcinomas and perhaps other types of human cancer.

183 **Overexpression of the WW domain of SETD2 inhibits pathways regulated by the**
184 **alternative RNA splicing of *U2AF2.***

185 The exon 2-defficient splice variant of *U2AF2,* which is expressed in shIWS1 and
186 shIWS1/MT-R cells, is defective in the processing of the *CDCA5* pre-mRNA. This results in
187 the downregulation of the *CDCA5* protein product, Sororin. The latter is involved in the
188 regulation of ERK phosphorylation, the expression of CDK1 and Cyclin B1, and the regulation
189 of the G2/M phase of the cell cycle (Laliotis et al., 2021[3]). Cells expressing the exon 2-deficient

190 *U2AF2* are also defective in the nucleocytoplasmic transport of the mRNAs of a set of
191 intronless genes that harbour CAR-Elements, including *JUN*, *HSBP1* (encoding HSP27),
192 *IFNA1* and *IFNB1* (encoding IFNα1 and IFNβ1 respectively) (Laliotis et al., 2021[8]). We
193 therefore asked whether, by promoting the skipping of *U2AF2* exon 2, the overexpression of
194 the WW domain of SETD2 also inhibits the phosphorylation of ERK and the expression of
195 CDK1 and Cyclin B1, as well as the expression and ERK-dependent phosphorylation of JUN,
196 and the expression of HSP27 and type I IFNs. The results confirmed the prediction by showing
197 that the WW domain of SETD2 reproduces the IWS1 knockdown ERK phosphorylation, cell
198 cycle and RNA transport phenotypes (**Fig. 4a, 4b**). Type I IFNs in this experiment were
199 induced by Sendai virus infection (Laliotis et al., 2021[8]) (**Fig. 4b**).

200 Collectively, these results show that overexpression of the SETD2 WW domain inhibits
201 the endogenous IWS1/SETD2 interaction (**Fig. 2**), the binding of SETD2 and the abundance
202 of H3K36me3 marks in select regions of target genes, the IWS1 dependent-alternative RNA
203 splicing of the targets of the IWS1 phosphorylation pathway (**Fig. 3)**, and signalling pathways
204 controlled by these targets (**Fig. 4**).

205 **Overexpression of the SETD2 WW domain inhibits cell cycle progression and**
206 **proliferation of lung adenocarcinoma cell lines, and anchorage-independent growth of**
207 **Human Bronchial Epithelia Cells (HBECs) transduced with IWS1-S720D/T721E**
208 **(IWS1/DE).**

209 Our earlier studies had shown that the IWS1 phosphorylation pathway is cell cycle-
210 regulated, and that its inhibition profoundly affects the proliferation of lung adenocarcinoma
211 cell lines. Given that the overexpression of the SETD2 WW domain inhibits this pathway, we
212 examined its effects on the proliferation of four lung adenocarcinoma cell lines (NCI-H522,
213 NCI-H1299, A549 and NCI-H1975) in culture. The same cells transduced with shIWS1 were
214 used as controls. The results showed that the proliferation of 2D cultures of all four cell lines
215 was significantly impaired when the cells were transduced with a lentiviral construct of the WW
216 domain (**Fig. 5a** and **Supplementary figure 1a**). Flow-cytometric analysis of log phase

217 cultures of NCI-H522, NCI-H1299, A549 and NCI-H1975 cells transduced with shControl,
218 shIWS1 or pLx304-SETD2/WW constructs and stained with Propidium Iodide (PI), confirmed
219 that the overexpression of the WW domain of SETD2 results in partial G2/M arrest, as
220 expected (**Fig. 5b**).

221 To determine whether the partial G2/M arrest and the inhibition of cell proliferation by
222 the overexpressed WW domain of SETD2 are because of the overexpression on the
223 alternative RNA splicing of *U2AF2*, we examined the ability of the RS domain-containing
224 U2AF65α and the RS domain-deficient U2AF65β to rescue the hypo-proliferative phenotype
225 induced by the overexpression of the WW domain. The results confirmed that whereas
226 U2AF65α rescues the phenotype, U2AF65β does not (**Supplementary Fig. 1b and Fig. 5c**).
227 However, the rescue was only partial, suggesting that overexpression of the WW domain of
228 SETD2 may inhibit cell proliferation by targeting the alternative RNA splicing of *U2AF2*, in
229 addition to other targets, which have not been identified to-date.

230 In parallel experiments, we overexpressed the SETD2 WW domain in human bronchial
231 epithelial cells immortalized with the telomerase catalytic subunit hTERT, (hTERT-HBEC) and
232 transformed with the constitutively active phosphomimetic mutant IWS1-DE. hTERT-HBECs
233 transduced with the empty vector pLx304, were used as controls. The soft agar colony growth
234 data in these cells showed that the WW domain inhibits anchorage-independent cell growth
235 (**Fig 5d**). These data were consistent with the proliferation data in the lung adenocarcinoma
236 cell lines, described in the preceding paragraph.

237

238 **Overexpression of the SETD2 WW domain blocks the IWS1 phosphorylation pathway**
239 **and inhibits the growth of NCI-H1299 mouse xenografts.**

240 The data in the preceding paragraphs confirmed that the inhibition of cell proliferation and
241 transformation by the SETD2 WW domain is due, at least in part, to the inhibition of the pIWS1
242 /*U2AF2* /*CDCA5* pathway, which based on our earlier observations, is strongly pro-oncogenic
243 (Laliotis et al., 2021[3]). This raised the question whether the SETD2 WW domain peptide
244 inhibits the growth of lung adenocarcinoma mouse xenografts. The experiment addressing

245 this question was done, using two groups of NSG (NOD.Cg-*Prkdc*^{scid} *Il2rg*^{tm1Wjl}/SzJ) mice (**Fig.**
246 **6a**). Group 1 was inoculated subcutaneously in the flanks with NCI-H1299 cells transduced
247 with a lentiviral shIWS1 construct, or with the empty lentiviral vector (shControl) (7 mice each,
248 14 mice total). Group 2 was inoculated similarly with NCI-H1299 cells transduced with the
249 same shIWS1 lentiviral vector used in group 1, or with a SETD2 WW domain construct in the
250 lentiviral vector pLx304 (also 7 mice each, 14 mice total) (**Fig 6a**). The animals were
251 monitored for tumor growth, and they were sacrificed 4 weeks later. The results confirmed that
252 both the loss of IWS1 and the overexpression of the SETD2 WW domain, significantly reduce
253 tumor growth. Notably, the inhibition of tumor growth in mice inoculated with NCI-H1299 cells
254 engineered to overexpress the SETD2 WW domain was more robust than the inhibition of
255 tumor growth in mice inoculated with shIWS1-transduced cells (**Fig. 6b**). This observation
256 supports the hypothesis that the SETD2 WW domain may inhibit cell proliferation by targeting
257 not only the alternative RNA splicing of *U2AF2*, but also other cell proliferation-promoting
258 targets.

259 Based on the preceding data and the role of the IWS1 phosphorylation pathway in
260 tumor cell proliferation in culture and in animals (Sanidas et al., 2014[2], Laliotis et al., 2021[3]
261 and this report), we hypothesized that the WW domain of SETD2 would inhibit the interaction
262 of IWS1 with SETD2 in mouse xenografts, and by inhibiting the interaction, would also inhibit
263 xenograft growth. This was confirmed with co-immunoprecipitation experiments, which
264 showed that overexpression of the SETD2 WW domain indeed inhibits the interaction between
265 IWS1 and SETD2 (**Fig. 6c**). The expression of the SETD2 WW domain and the abundance of
266 IWS1 and phosphor-IWS1 in these tumors, were confirmed by western blotting (**Fig. 6d**).
267 Using RT-PCR we also addressed the alternative RNA splicing of confirmed targets of the
268 IWS1 phosphorylation pathway. The results showed that in mouse xenografts, like in cultured
269 cells, overexpression of the SETD2 WW domain dramatically inhibits the IWS1
270 phosphorylation-dependent alternative RNA splicing pathway (**Fig. 6d**). Next, we probed
271 western blots of tumor cell lysates with antibodies to Sororin, phosphor-ERK (Y202/T204),
272 CDK1, Cyclin B1, PCNA and Ki-67, all of which are regulated by the IWS1 phosphorylation-

273 dependent alternative RNA splicing of *U2AF2* (Laliotis et al., 2021[3]). The results confirmed
274 that the WW domain also inhibits the phosphorylation of ERK and the expression of these
275 regulators of the cell cycle (**Fig. 6d**). We conclude that overexpression of the SETD2 WW
276 domain inhibits tumor growth, by inhibiting the IWS1/U2AF2/CDCA5 pathway and cell cycle
277 progression.

278 IWS1 phosphorylation controls the alternative RNA splicing of *FGFR2*, favoring the
279 *FGFR2* mRNA splice variant IIIc. This variant is expressed primarily in mesenchymal cells,
280 and it has been shown to promote epithelial to mesenchymal transition (EMT) in cancer cells.
281 We therefore questioned whether the overexpression of the SETD2 WW domain inhibits the
282 expression of EMT markers in the developing tumors. Immunohistochemistry experiments,
283 addressing the expression of ZEB1, TWIST and Vimentin confirmed this prediction (**Fig. 6d**).

284 Representative examples of the histology of the tumors derived from shControl,
285 shIWS1 and pLx304-SETD2 WW domain-transduced NCI-H1299 cells (**Fig. 6e)**. The same
286 figure also shows representative examples of immunohistochemistry experiments addressing
287 the expression of the Ki-67 proliferation marker, ZEB1, TWIST and Vimentin in the same
288 tumors. Whereas the histology of the tumors derived from the control cells was similar to the
289 histology of the tumors derived from cells engineered to express the WW domain of SETD2,
290 the results of the Ki-67 ZEB1, TWIST and Vimentin immunohistochemistry experiments
291 revealed that overexpression of the WW domain of SETD2, resulted in the downregulation of
292 all these markers (**Fig. 6e**). Quantification of the abundance of Ki-67 ZEB1, TWIST and
293 Vimentin in all the same tumors confirmed the results (**Fig. 6f**) and was consistent with the
294 western blot data (**Fig. 6d)**.

295 Overall, the data in this report support the model in figure 7. According to this model,
296 the SETD2 WW domain binds phosphorylated IWS1, and by doing so it antagonizes the
297 interaction of phosphor-IWS1 with SETD2 and the recruitment of SETD2 to the RNA
298 elongation complex assembling on the Ser2-phosphorylated CTD of RNA Pol II. Blocking the
299 recruitment of SETD2 to the complex prevents histone H3K36 trimethylation in the body of
300 target genes during transcriptional elongation. Given the importance of H3K36me3 marks in

301 RNA elongation and RNA processing, the loss of these marks results in major shifts in RNA
302 splicing and other RNA processing events. This alters the IWS1 phosphorylation-dependent
303 H3K36me3 distribution and subsequent oncogenic AKT/IWS1 RNA splicing program, leading
304 to inhibition of tumor growth (**Fig. 7**).

305 In addition to showing that blocking the interaction of phosphor-IWS1 with SETD2 is
306 feasible and has profound effects on the biology of tumor cells, the data in this report also
307 provide information for the design of a strategy to screen for small molecules to inhibit the
308 interaction. Such molecules hold promise for the therapeutic targeting of the AKT/phosphor-
309 IWS1 pathway in lung adenocarcinomas and potentially other types of human cancer.

310

311 **Discussion**

312 Although AKT is known to play a major role in most types of human cancer, its
313 therapeutic targeting has been only minimally successful to-date. This may be due to several
314 reasons. First, there are three AKT isoforms which functionally overlap, but also have non-
315 overlapping, and in some cases opposing functions (Song et al., 2019[10], Wang et al., 2018[11]).
316 This suggests that using inhibitors that target all AKT isoforms, which is the case for most of
317 the inhibitors available to-date, may have suboptimal results. Another reason is that AKT has
318 wide reaching effects in cell signalling, both in normal and in cancer cells (Manning et al.,
319 2017[12]), and its inhibition may result in significant toxicity. One way to address these limitations
320 is to identify and selectively target AKT-regulated signalling pathways with critical roles in
321 human cancer. One such pathway is the IWS1 phosphorylation pathway, which is activated
322 by AKT in a cell cycle-dependent manner and epigenetically regulates transcription, RNA
323 metabolism and perhaps other epigenetically regulated processes, and has a major role in
324 human lung adenocarcinomas and most likely in other forms of human cancer (Sanidas et al,
325 2014[2], Laliotis et al, 2021[3]). In this report we present our initial data on a strategy aiming to
326 selectively target this pathway.

327 The knockdown of IWS1 in human lung adenocarcinoma cell lines, and its rescue with
328 the S720A/T721A IWS1 mutant, which cannot be phosphorylated by AKT, result in significant

329 inhibition of cell proliferation in culture and tumor growth in xenograft models in
330 immunocompromised mice. Our recent studies provided a mechanistic explanation for this
331 observation, by showing that IWS1 is induced and undergoes phosphorylation by AKT during
332 the transition from the G1 to the S phase of the cell cycle, and that following phosphorylation,
333 it regulates the alternative RNA splicing of multiple genes, one of which is *U2AF2,* the gene
334 encoding the core RNA splicing factor U2AF65. The predominant *U2AF2* mRNA in cells with
335 low abundance of phosphorylated IWS1 lacks exon 2, which encodes the RS domain of
336 U2AF65, a domain that is required for the interaction of U2AF65 with additional RNA splicing
337 regulators, including Prp19. The loss of the Prp19-interacting domain impairs the recruitment
338 of the Prp19 complex (Prp19C) to the spliceosome, resulting in defects in the processing and
339 nucleocytoplasmic transport of the mRNAs of multiple genes. One of these genes is *CDCA5,*
340 which encodes Sororin, a member of the Cohesin complex (Zhang et al., 2012[13]). The IWS1-
341 regulated Sororin is phosphorylated by ERK and the phosphorylated Sororin enhances ERK
342 phosphorylation by an unknown mechanism. This Sororin/ERK feedback loop promotes
343 progression through the G2/M phase of the cell cycle and cell proliferation (Laliotis et al,
344 2021[3]).

345 As indicated above, the IWS1 phosphorylation-dependent alternative RNA splicing of
346 *U2AF2* also regulates the nucleocytoplasmic transport of the mRNAs of a set of intronless
347 genes, which harbor Cytoplasmic Accumulation Region Elements (CAR-E). The absence of
348 IWS1 phosphorylation therefore, lowers the nuclear export of these mRNAs and the
349 abundance of the proteins they encode. Genes, whose regulation by this mechanism has been
350 confirmed, include *JUN*, *HSPB1* (encoding Hsp27), *IFNA1* and *IFNB1* (encoding IFNα1 and
351 IFNβ1 respectively). The abundance of these proteins may affect cell proliferation and survival
352 in response to external signals, in addition to regulating the sensitivity to viral infection (Laliotis
353 et al., 2021[8]).

354 *FGFR2* is also known to undergo alternative RNA splicing and our earlier studies had
355 shown that its RNA splicing is also regulated by IWS1 phosphorylation. The latter promotes
356 the skipping of exon 8, giving rise to the IIIc mRNA transcript, which is observed in

357 mesenchymal cells and is associated with Epithelial to Mesenchymal Transition (EMT). The
358 loss of IWS1 phosphorylation on the other hand, promotes the inclusion of exon 8, giving rise
359 to the IIIb mRNA transcript of *FGFR2*, which is observed in epithelial cells. By regulating the
360 alternative RNA splicing of *FGFR2*, the IWS1 phosphorylation pathway also promotes EMT,
361 cell migration and tumor cell invasiveness. By regulating these pathways, IWS1
362 phosphorylation contributes to cell transformation in culture and to tumor growth in animals.
363 More important, this pathway is active in human lung adenocarcinomas, especially those with
364 EGFR mutations, and the activity of the pathway correlates with tumor stage, histologic grade,
365 metastasis, relapse after treatment, and poor prognosis.

366 The first step in the activation of the IWS1 pathway is the recruitment of SETD2 to an
367 SPT6/IWS1/ALY-REF complex, which assembles on the Ser2-phosphorylated CTD of RNA
368 Pol II. The signal for the recruitment of SETD2 is the phosphorylation of IWS1 by AKT. The
369 work presented in this report focuses on the question whether we can block the interaction
370 between phosphorylated IWS1 and SETD2 and whether blocking this interaction will result in
371 the reversal of the known phenotypic effects of the pathway in cancer cells. Using deletion
372 mutants of SETD2 and co-immunoprecipitation assays in HEK293 cells we mapped the IWS1-
373 interacting domain of SETD2 to its WW domain, a short, 33 amino-acid peptide. The SETD2
374 WW domain is preceded by a proline-rich stretch and the same is observed in the WW
375 domains of other proteins, including Huntingtin. NMR studies of the Huntingtin WW domain
376 have shown that it interacts with the proline-rich stretch, and that the interaction between the
377 two domains results in a closed conformation (Gao et al., 2014[14]). If the interaction between
378 these domains is conserved in SETD2 as expected, it may have an auto-inhibitory role. In this
379 case, the binding to phosphorylated IWS1, may allosterically activate SETD2. This finding is
380 significant because it suggests that the binding of SETD2 to the CTD complex does not only
381 link SETD2 to the machinery that will allow it to methylate chromatin during transcriptional
382 elongation, but that it may also activate it.

383 The WW domain is defined by the presence of two tryptophan (W) residues 20-23 aa
384 apart (Vargas et al., 2019[15], Jäger et al., 2006[16]). WW domains bind proline-rich protein

385 regions, including proline-rich phosphor-tyrosine and phosphor-serine-threonine sites (Ingham
386 et al., 2005[17], Sudol et al., 2010[18], Salah et al., 2012[19]). By binding to their targets, they
387 transduce signals along signalling cascades and they regulate the cytoskeleton and cell
388 polarity (Lin et al., 2019[20], Ilsley et al., 2002[21]). Changes in the interaction between WW
389 domains and their targets have been linked to genetic disorders, such as the Liddle syndrome
390 (Pucheta-Martinez et a., 2016[22], Chang et al., 2019[23], Sudol et al., 2012[24]) muscular dystrophy,
391 Huntington's chorea, Alzheimer's disease (Kunkle et al., 2019[25]) and cancer (Salah et al.,
392 2011[26], Lee et al., 2012[27], Hung et al., 2020[28]). Based on the motifs they bind, five classes of
393 WW domains have been identified to-date. The most common is Class I, which recognizes
394 the sequence (L/P)Pp(Y/poY), where L and P stand for Leucine and Proline respectively,
395 identifies a phosphorylated residue and lower case letters represent favoured, but not
396 conserved residues (Salah et al., 2012[19]). The IWS1 domain interacting with SETD2 extends
397 from amino acid 522 to amino acid 698 (Yoh et al., 2008[9]). Analysis of this sequence identified
398 several Class I and Class II motifs, which may be recognized by the WW domain of SETD2
399 (**Supplementary Fig. 2**). However, the role of these motifs in the phosphor-IWS1/SETD2
400 interaction remains to be determined.

401 Data in figure 5 showed that the proliferation defect induced by the overexpression of
402 the WW domain of SETD2 in lung adenocarcinoma cell lines is rescued, but only partially, by
403 the RS domain containing U2AF65 isoform, U2AF65α. Moreover, the data in figure 6, showed
404 that the growth inhibition of tumor xenografts engineered to overexpress the WW domain of
405 SETD2, is more robust than the growth inhibition induced by the IWS1 knockdown. These
406 data combined, suggest that the overexpression of the WW domain of SETD2 may inhibit cell
407 proliferation by targeting the alternative RNA splicing of *U2AF2*, in addition to other targets
408 that have not been identified to-date. p53, which interacts with the WW domain of SETD2 via
409 its N-terminal transactivation domain (aa 1-45) is unlikely to be one of these targets, because
410 its interaction with SETD2 stimulates the expression of many of the anti-proliferative and pro-
411 apoptotic genes it regulates (Xie et al, 2008[29]). Therefore, blocking its interaction with SETD2
412 should inhibit the expression of these genes. In addition, p53 should not be relevant to some

of the cell lines we used in this study, including NCI-H1299, which is p53-null, and perhaps NCI-H522 and NCI-H1975, which harbor point mutations in p53. Another protein known to interact with the WW domain of SETD2 is Huntingtin (Gao et al., 2014[14], Seervai et al., 2020[30]). SETD2 bound to Huntingtin and the actin-binding adaptor HIP1R, trimethylates Actin at K68. ActK68me3 localizes to the F-actin cytoskeleton and regulates actin polymerization/depolymerisation. Blocking actin methylation, which is expected to occur in cells overexpressing the WW domain of SETD2, inhibits cell migration (Seervai et al., 2020[30]) and perhaps cell survival (Cisbani et al., 2012[31]).

In summary, data presented in this report, provide robust evidence that selective inhibition of the IWS1 phosphorylation pathway has a strong therapeutic potential. In addition, they show that blocking the interaction between phosphorylated IWS1 and SETD2 is feasible and it can effectively inhibit the pathway. Finally, they provide a roadmap for strategies that can be employed to identify small molecule inhibitors of the pathway.

426 **Methods**

427

428 **Cells and Culture conditions.**

429 NCI-H522, NCI-H1299, A549, NCI-H1975 and HBEC-hTERT cells were grown in Roswell
430 Park Memorial Institute 1640 medium (Sigma-Millipore, Cat No. D8758) and HEK-293T cells
431 were grown in Dulbecco's modified Eagle's medium (Sigma-Millipore, Cat No. D5796)
432 supplemented with penicillin/streptomycin (Corning, Cat No. 30-002-CI), nonessential amino
433 acids (Corning, Cat No. 25-025-CI), glutamine (Corning, Cat No. 25-005-CI), plasmocin
434 2.5ng/uL (Invivogen, Cat No. ant-mpp) and 10% fetal bovine serum. Cells were used for up to
435 5 passages. Cell lines were also periodically checked for mycoplasma, using the PCR
436 mycoplasma detection kit (ABM, Cat No. G238). All experiments were carried out in
437 mycoplasma-free cultures.

438 **shRNAs and expression constructs**

439 The origin of the shRNAs and expression constructs is described in Supplementary Table 3.
440 The SETD2 deletion mutants were cloned in pENTR/D-TOPO cloning vector (Invitrogen, Cat.
441 No. 45-0218), with PCR-based techniques, using pENTR SETD2-HA wt clone as substrate
442 (Open Biosystems MHS6278-211691086, Clone ID : 40125713, corresponding to
443 NM_014159.6, Sanidas et al., 2014[2], Laliotis et al., 2021[3]). To ensure successful amplification
444 and separation, the PCR products were run in 1% agarose gel and were gel-purified using the
445 NucleoSpin Gel and PCR Clean-Up kit (M&N, Cat. No. 740609.50). Following cloning in the
446 entry vector, the two clones were recombined with Gateway™ pcDNA™-DEST40 Vector
447 (Thermofisher, Cat No #12274015) for transient transfection or with the pLx304 V5-DEST
448 (Addgene #25890) for stable expression, using standard Clonase II LR mix (Thermofisher, Cat
449 No 11791100). The retroviral expression vector for the two U2AF65 isoforms was created by
450 recombining pENTR U2AF65 (α or β isoform) (Laliotis et al., 2021[3]), with pMSCV N-Flag-HA
451 IRES puro (Addgene #41033). Using Clonase II LR as well. The primers used for the cloning
452 are listed in Supplementary Table 3. All constructs were sequenced in Genomic Shared
453 Resource of The Ohio State University, prior to use.

454
455 **Transfections and infection**

456 Retroviral constructs were packaged by transient transfection of these constructs in HEK-293T
457 cells, in combination with ecotropic (Eco-pac) or amphotropic (Ampho-pac) packaging
458 constructs. Lentivirus constructs were also packaged in HEK-293T cells by transient
459 transfection of the constructs in combination with the packaging constructs psPax2 (Addgene
460 #12260) and pMΔ2.G (Addgene #12259). Transfections were carried out using 2x HEPES
461 Buffered Saline (Sigma, Cat. No 51558) and $CaCl_2$ precipitation.After 48 hours of transient
462 transfections of HEK-293T cells, the supernatant were collected and filtered. Infections were
463 carried out in the presence of 8 µg/ml polybrene (Sigma, Cat. No. 107689). Depending on the
464 selection marker in the vector, 48 hours after the infection, cells were selected for resistance
465 to puromycin (Gibco, Cat. No. A11138) (10 µg/ml), G-418 (Cellgro, Cat. No. 30-234)
466 (500µg/ml), or blasticidin (Gibco, Cat. No A1113903) (5 µg/ml). Cells infected with multiple
467 constructs, were selected for infection with the first construct, prior to the next infection. The
468 transient transfection of the HA-SETD2 deletion mutants in NCI-H522 and NCI-H1299 were
469 performed using 2x HEPES Buffered Saline and $CaCl_2$ precipitation. After 48 hours the cells
470 were harvested.

471 **Virus propagation, titering and infections**

472 For the stimulation of the type I IFN, the NCI-H522 and NCI-H1299 were subjected to infection
473 with Sendai-GFP (SeV-GFP) (Yount et al., 2006[32]), as previously described (Laliotis et al.,
474 2021[8]). Briefly, the cells were infected by using an MOI=0.5 for 16h and MOI of 0.25 for 24h,
475 respectively. Sendai virus expressing GFP (SEV-GFP) was propagated in 10-day-old
476 embryonated chicken eggs at 37°C for 40 hours and titered on Vero cells.

477 **Cell Proliferation assay**

478 The cell proliferation assay was performed as previously described (Laliotis et al., 2021[3]).
479 Briefly, the cells were harvested by trypsinization, counted and plated evenly in 12 well tissue

480 culture plates in 3 biological replicates for each condition. For all the cells and conditions 5,000
481 cells/well were plated. Photomicrographs were taken every 6 hours using an Incucyte live cell
482 imager (Essen Biosciences, Ann Arbor, MI) depending on growth parameters of each cell line
483 (NCI-H522 7 days, NCI-H1299 7 days, A549 7 days and NCI-H1975 12 days total acquisition).
484 Images were taken and analyzed using the Incucyte confluence masking software (Essen
485 Biosciences, Ann Arbor, MI)

486 **Cell Transformation assay**

487 The cell transformation assay was performed and analyzed as previously described (Laliotis
488 et al., 2021[3]), using the Cell Transformation Assay Kit-Colorimetric (Abcam Cat No.
489 ab235698). Briefly, $1x10^4$ HBEC hTERT cells per condition were mixed with top agarose layer
490 in 10x DMEM solution and plated in 96-well plate, in triplicates along with three blank wells.
491 The cells were then plated for 7 days in 37°C and monitored for colony formation. After 7 days,
492 the cells were imaged in the Incucyte live cell imager using the 20x lens. Then, the cells were
493 incubated for 4 hours on WST working solution at 37°C. The absorbance at 450nm was
494 determined with a plate reader.
495

496 **FACS analysis**

497 The FACS assays was performed and analysed as previously described (Laliotis et al., 2021[3]).
498 Briefly, the cells were plated in equal numbers and they were harvested from semi-confluent
499 cultures 48 hours later. The cellular pellet was resuspended in 700uL ice-cold 1x PBS and
500 fixed in 2.8mL ethanol, overnight at -20°C. Following two washes with 1x PBS, the fixed cells
501 were stained with Propidium Iodide mix (Propidium Iodide (1:2500) (Invitrogen, Cat. No.
502 P3566), 0.1 mg/mL RNAse A (Invitrogen, Cat. No. 12091-039), 0.05% Triton-X) and incubated
503 in the dark at 37°C for 30 minutes. Subsequently, the cells were analysed on the BD
504 FACSCalibur (BD Biosciences, San Jose, CA). The analysis was performed in the Flow
505 Cytometry Shared Resource (FCSR) of the Ohio State University.

506 **RT-PCR and qRT-PCR**

507 Total cell RNA was extracted using the PureLink RNA Kit (Invitrogen, Cat. No 12183018A),
508 as previously described (Laliotis et al., 2021[3]). Briefly, cDNA was synthesized using oligo-dT
509 priming and the QuantiTect Rev. Transcription Kit (QIAGEN, Cat No. 205310) and the gene
510 and exon expressions were quantified by quantitative real time RT-PCRusing the iTaq™
511 Universal SYBR® Green Super mix (Biorad, Cat No. 1725121) and a StepOne Plus qRT-PCR
512 machine (Thermofisher). Data was normalized to hGAPDH or human 18S rRNA, which was
513 used as an internal control. The primer sets used for all the real time PCR assays throughout
514 this report are listed on the Supplementary Table 2.

515

516 **Western Blotting**

517 Western blotting was performed as previously described (Laliotis et al., 2021[3]). Briefly, the
518 cells were lysed using a RIPA lysis buffer (50 mM Tris (pH 7.5), 0.1% SDS, 150 mM NaCl, 5
519 mM EDTA, 0.5% Sodium deoxycholate, 1% NP-40 and fresh 1x Halt™ Protease and
520 Phosphatase Inhibitor Cocktails (Thermofisher, Cat. No 78444). The clarified lysates were
521 electrophoresed (20μg protein per lane) in SDS-PAGE. Electrophoresed lysates were
522 transferred to polyvinylidene difluoride (PVDF) membranes (EMD Millipore Cat No.
523 IPVH00010) in 25 mM Tris and 192 mM glycine. The membranes were probed with antibodies
524 (at the recommended dilution), followed by horseradish peroxidase-labeled secondary
525 antibodies (1:2500), and they were developed with Pierce ECL Western Blotting Substrate
526 (Thermo Scientific, cat. no 32106). The antibodies used are listed in Supplementary Table 1.

527 **Immunoprecipitation**

528 Immunoprecipitation assays was performed as previously described (Laliotis et al., 2021[3]).
529 Briefly, cells were lysed using a cytosolic Lysis Buffer 1 (LB1), Lysis Buffer 2 (LB2) and nuclear

530 Lysis Buffer 3 (LB3). Following overnight incubation with the immunoprecipitating antibody
531 (Supplementary Table 1) or the rabbit Isotype Control (Thermofisher, Cat. No 10400C) at 4°C,
532 the conjugates were subjected to multiple washes with LB3 and 300uL of the clarified lysates
533 were added in the Magnetic beads-Antibody conjugates, followed by overnight incubation at
534 4°C. Following several washes with LB3, they were electrophoresed (20µg protein per lane)
535 in SDS-PAGE, as described in Western Blotting section.

536 **Image acquisition and figure preparation**

537 For the western blotting images, the acquisition was performed in Li-Cor Fc Odyssey Imaging
538 System (LI-COR Biosciences, Lincoln, NE) using the 700 nm (protein ladder detection), 800
539 nm (reduced background and increased sensitivity) and chemi luminescent (protein bands)
540 detection using a linear acquisition method. For the DNA agarose gels, the acquisition was
541 performed in Li-Cor Fc Odyssey Imaging System using the 600 nm channel using a linear
542 acquisition method. Identical approach was followed for all the images presented in this report
543 to ensure unbiased analysis. In both conditions, the images were exported in high-quality
544 image files (600 dpi png files) and further imported in Adobe Illustrator 2021 (Adobe, San Jose,
545 CA) for figures preparation. The summary figures were designed in Bio Render
546 (https://biorender.com).

547 **Chromatin Immuno-Cleavage (ChIC)**

548 In order to address the SETD2 and H3K36me3 abundance of IWS1-dependent targets, we
549 utilized ChIC assays as previously described (Laliotis et al., 2021[3], Skene et al 2013[33]). Briefly,
550 $2.5x10^5$ cells were washed several times with wash buffer. Magnetic Biomag Plus
551 Concanavalin A Beads (Bangs Laboratories, Cat. No. BP531) were activated with multiple
552 washes using a binding buffer. Prior to use, the immunoprecipitation antibodies
553 (Supplementary Table 1) or the Rabbit Isotype Control (Thermofisher, Cat. No 10500C), were
554 diluted in 1:50 dilution in 50 uL antibody buffer]. Then, the activated beads were resuspended
555 with the antibody buffer, containing the immunoprecipitated antibody, and mixed with the cell

556 fraction. Following overnight incubation at 4°C, the immunoprecipitates were subjected to
557 multiple washes with the wash buffer. Similarly to the primary immunoprecipitating antibody,
558 the Guinea Pig anti-Rabbit IgG (Heavy & Light Chain) secondary antibody (Antibodies-Online,
559 Cat. No. ABIN101961) was diluted in 1:50 dilution in 50uL antibody buffer, was mixed with the
560 immunoprecipitates. Subsequently, the immunoprecipitates were subjected to multiple
561 washes and mixed with the CUTANA™ pAG-MNase (EpiCypher, Cat No. SKU: 15-1116) at
562 700 ng/mL. The targeted digestion was activated with 100mM $CaCl_2$ and occurred by
563 incubation on ice for 30 minutes. The reaction was terminated with addition of 2x stop buffer
564 and the chromatin fragments were released by incubation at 37°C for 10 minutes.
565 Subsequently, the chromatin fragments were extracted with DNA Purification Buffers and Spin
566 Columns (Cell SIgnaling, Cat. No 14209). Real-time PCR using different sets of primers to
567 amplify the genomic loci was carried out as described in the qRT-PCR section. The data were
568 analysed using the analysis substrate file provided online by Sigma-Aldrich, calculating the
569 fold enrichment. (https://www.sigmaaldrich.com/technical-documents/articles/biology/chip-
570 qpcr-data-analysis.html).

571 **Tumor xenografts**

572 *Ethics statement:* All experimental procedures were approved by the Institutional Animal Care
573 and Use Committee (IACUC) of the Ohio State University. IACUC protocol number
574 2018A00000126; P.I.: Philip Tsichlis.

575 *Procedure:* The mouse xenograft engraftment was performed as previously described (Laliotis
576 et al., 2021[3]). 2x10^6 NCI-H1299 cells per injection were mixed with 30% Matrigel (Corning,
577 Cat. No. 356231) in PBS for a total volume of 200 µl and implanted subcutaneously into either
578 side (left side for the shControl and right side for the shIWS1 group 1 and lift side for the
579 shIWS1 and right side for the pLx304 SETD2 WW group 2) of immunocompromised 6 week
580 old NSG (NOD.*Cg-Prkdc*^{scid} *Il2rg*^{tm1Wjl}/SzJ) female mice. The mice were monitored every 3
581 days and the size of the tumors was measured using a digital caliper. The tumor volume was
582 calculated by use of the modified ellipsoid formula: $\underline{V} = \frac{1}{2}\ \nu \times s^2$ (1/2 Length × Width^2). The
583 mice were sacrificed 4 weeks after the injection. The tumors were removed and their weights
584 were measured. One part of the dissected tumors was immediately snap frozen in liquid
585 nitrogen prior to RNA and protein isolation, and a second part was fixed overnight in 10% (v/v)
586 formalin (Sigma, Cat. No. HT501640), transferred to 70% EtOH and then embedded in paraffin
587 at the Comparative Pathology & Mouse Phenotyping Shared Resource of the Ohio State
588 University Comprehensive Cancer Center, prior to immunohistochemistry (IHC) staining.

589 **RNA and protein isolation from the mouse xenograft tumors**

590 The RNA and protein extraction from the mouse tumors was performed as previously
591 described (Laliotis et al., 2021[3]). Briefly, 50-100 mg of the frozen mouse xenograft samples
592 were homogenized using 1mL Trizol reagent (Thermofisher Scientific, Cat. No. 15596026).
593 RNA and protein were extracted according to the manufacturer's instructions. Both protein
594 and RNA materials from the tumors were further processed with immunoblotting and qRT-
595 PCR, respectively, for the expression of various targets described in this report.

596 **IHC staining**

597 The IHC staining from the mouse tumors was performed as previously described (Laliotis et
598 al., 2021[3]). Briefly, sections of 5 μm from the paraffin embedded mouse tumors were heated
599 to 55°C for 20 min prior to deparaffinization in xylene (Fisher scientific, Cat. No. X3F-1GAL).
600 The slides were then rehydrated through graded ethanol concentrations up to distilled water.
601 The endogenous peroxidase activity was blocked at RT by a 10 min incubation in the final
602 developmental 3% H_2O_2 (Fisher Scientific, Cat. No. H325500) in PBS (pH 7.4), followed by
603 antigen retrieval at 80 °C for 30min using the Citrate Buffer, pH 6.0, Antigen Retriever (Sigma,
604 Cat. No. C9999). The Vectastain Elite ABC Universal kit peroxidase (Horse Anti-Mouse/Rabbit
605 IgG) (Vector Laboratories, Cat. No. PK-6200) was used for blocking and incubation with the
606 primary and secondary antibody according to the manufacturer's instructions. After a 5 min
607 wash with 1x PBS the slide was incubated for 30 min with the Vectastain Elite ABC reagent
608 followed by a 2-10 min incubation with a DAB peroxidase substrate solution (Vector
609 Laboratories, Cat. No. SK-400) according to the manufacturer's instructions. The slide was
610 then washed in tap water and covered with the DPX mounting medium (Sigma, Cat. No.
611 06522).

612 **Imaging**

613 All images were captured on the Nikon eclipse 50i microscope with attached Axiocam 506
614 color camera using the ZEN 2.6 blue edition software (Zeiss). Image processing and analysis
615 was further performed using the ImageJ software, as described in the following section.

616 **Analysis of IHC signal**

617 Imaging files were imported to ImageJ (Schneider et al., 2012[45]) and analyzed as previously
618 described (Laliotis et al., 2021[3]). For each slide, at least 5 different areas of the tumor were
619 scanned. The average value of the signal divided to its different area, was the final value of

620 the analysis. Identical approach and settings were followed for all the images to ensure
621 unbiased analysis.

622 **Data availability**

623 All the raw data underlying figures 1-6 (uncropped gel images, qPCR, FACS, plates reader
624 and proliferation data) and microscope images derived from this report have been deposited
625 in the Mendeley Dataset in a publicly available dataset (Laliotis et al., 2021[35]). Specific *P*
626 values are also included in these datasets.
627

628 **Statistics and reproducibility**

629 The experiments in Fig. 1b-c, 2a-2c, 4a-4b were performed twice. The experiments in Fig. 3a-
630 d and 5a-5d were performed at least in 3 independent biological experiments. The data in
631 figure 6 (mouse xenografts) were performed once, using 7 mice/group. The Western blot
632 analysis, IP experiments, RT-PCR assays and IHC staining of xenografts derived tumors was
633 performed once with the techniques outlined in the methods section. All the statistical analysis
634 was performed in GraphPad Prism 9.1, as described in the corresponding section. All the
635 statistical analysis reports can be found in the Mendeley dataset where the source data of this
636 report were deposited. (Laliotis et al., 2021[35])

637 **Acknowledgments**

638 The authors wish to thank all the members of the Tsichlis Lab for helpful discussions. We are
639 grateful to Dr Michael Freitas for the pcDNA™-DEST40 Vector. We also thank Dr Joal Beane
640 for reviewing the manuscript before the submission. This work was supported by the NIH grant
641 R01 CA186729 to P.N.T., the NIH grant R01 CA198117 to P.N.T and V.C, by start-up funds
642 from the OSUCCC to P.N.T. from the National Centre for Advancing Translational Sciences
643 grant KL2TR002734 to L.S. G.I.L was supported by the Pelotonia Post-Doctoral fellowship
644 from OSUCCC.

645 **Author Contributions**

646 **G.I.L.** Conceptualization, overall experimental design. Performed experiments, analysed the
647 data, prepared the figures and wrote the manuscript. **E.C.** Designed and performed the mouse
648 xenografts, protein and RNA extraction of mouse tumours, performed the mouse xenografts
649 staining studies and picture acquisition and edited the manuscript **V.A.** Designed, performed,
650 analysed the proliferation experiments and edited the manuscript **S.S.** Assisted in FACS
651 experiments **A.D.K.** Designed, optimized and performed the infection with Sendai virus and
652 edited the manuscript **A.K.K.** Performed RT-PCR experiments and assisted in cloning. **K.A.N**
653 Performed RT-PCR experiments and assisted and assisted in cloning. **S.A.** Assisted in the
654 design for SETD2 deletion mutants and edited the manuscript **J.S.Y** Advised on the viral strain
655 infection and edited the manuscript **L.S.** Advised on the design of experiments and edited the
656 manuscript. **P.N.T.** Conceptualization, overall experimental design, project supervision,
657 manuscript writing and editing.

658 **Competing Interests**

659 The authors declare no competing interests.

660 **Corresponding authors**

661 Correspondence to : Philip N. Tsichlis (lead contact) and Georgios I. Laliotis
662

663 **References**

664

665 1. Yoh, S.M., Cho, H., Pickle, L., Evans, R.M. and Jones, K.A., 2007. The Spt6 SH2
666 domain binds Ser2-P RNAPII to direct Iws1-dependent mRNA splicing and export.
667 *Genes & development*, *21*(2), pp.160-174.
668 2. Sanidas, I., Polytarchou, C., Hatziapostolou, M., Ezell, S.A., Kottakis, F., Hu, L., Guo,
669 A., Xie, J., Comb, M.J., Iliopoulos, D. and Tsichlis, P.N., 2014. Phosphoproteomics

670 screen reveals akt isoform-specific signals linking RNA processing to lung cancer.
671 *Molecular cell*, *53*(4), pp.577-590.

672 3. Laliotis, G.I., Chavdoula, E., Paraskevopoulou, M.D. *et al.* AKT3-mediated IWS1
673 phosphorylation promotes the proliferation of EGFR-mutant lung adenocarcinomas
674 through cell cycle-regulated *U2AF2* RNA splicing. *Nat Commun* 12, 4624 (2021).
675 https://doi.org/10.1038/s41467-021-24795-1

676 4. Luco, R.F., Pan, Q., Tominaga, K., Blencowe, B.J., Pereira-Smith, O.M. and Misteli,
677 T., 2010. Regulation of alternative splicing by histone
678 modifications. *Science*, *327*(5968), pp.996-1000.

679 5. Thiery, J.P. and Sleeman, J.P., 2006. Complex networks orchestrate epithelial–
680 mesenchymal transitions. *Nature reviews Molecular cell biology*, *7*(2), pp.131-142.

681 6. Chanarat, S. and Sträßer, K., 2013. Splicing and beyond: the many faces of the Prp19
682 complex. *Biochimica et Biophysica Acta (BBA)-Molecular Cell Research*, *1833*(10),
683 pp.2126-2134.

684 7. David, C.J., Boyne, A.R., Millhouse, S.R. and Manley, J.L., 2011. The RNA polymerase
685 II C-terminal domain promotes splicing activation through recruitment of a U2AF65–
686 Prp19 complex. *Genes & development*, *25*(9), pp.972-983.

687 8. Georgios I. Laliotis, Adam D. Kenney, Evangelia Chavdoula, Arturo Orlacchio, Abdul
688 K. Kaba, Alessandro La Ferlita, Vollter Anastas, Christos Tsatsanis, Joal D. Beane,
689 Lalit Sehgal, Vincenzo Coppola, Jacob S. Yount, Philip N. Tsichlis, bioRxiv
690 2020.12.26.424461, IWS1 phosphorylation by AKT kinase controls the
691 nucleocytoplasmic export of type I IFNs and the sensitivity of lung adenocarcinoma
692 cells to cytolytic viral infection, through *U2AF2* RNA splicing.
693 *https://doi.org/10.1101/2020.12.26.424461*

694 9. Yoh, S.M., Lucas, J.S. and Jones, K.A., 2008. The Iws1: Spt6: CTD complex controls
695 cotranscriptional mRNA biosynthesis and HYPB/Setd2-mediated histone H3K36
696 methylation. *Genes & development*, *22*(24), pp.3422-3434.

697 10. Song, M., Bode, A.M., Dong, Z. and Lee, M.H., 2019. AKT as a therapeutic target for
698 cancer. *Cancer research*, *79*(6), pp.1019-1031.
699 11. Wang, J., Zhao, W., Guo, H., Fang, Y., Stockman, S.E., Bai, S., Ng, P.K.S., Li, Y., Yu,
700 Q., Lu, Y. and Jeong, K.J., 2018. AKT isoform-specific expression and activation
701 across cancer lineages. *BMC cancer*, *18*(1), pp.1-10.
702 12. Manning, B.D. and Toker, A., 2017. AKT/PKB signaling: navigating the
703 network. *Cell*, *169*(3), pp.381-405.
704 13. Zhang, N. and Pati, D., 2012. Sororin is a master regulator of sister chromatid cohesion
705 and separation. *Cell cycle*, *11*(11), pp.2073-2083.
706 14. Gao, Y.G., Yang, H., Zhao, J., Jiang, Y.J. and Hu, H.Y., 2014. Autoinhibitory structure
707 of the WW domain of HYPB/SETD2 regulates its interaction with the proline-rich region
708 of huntingtin. *Structure*, *22*(3), pp.378-386.
709 15. Vargas, R.E., Duong, V.T., Han, H., Ta, A.P., Chen, Y., Zhao, S., Yang, B., Seo, G.,
710 Chuc, K., Oh, S. and El Ali, A., 2020. Elucidation of WW domain ligand binding
711 specificities in the Hippo pathway reveals STXBP 4 as YAP inhibitor. *The EMBO*
712 *journal*, *39*(1), p.e102406.
713 16. Jäger, M., Zhang, Y., Bieschke, J., Nguyen, H., Dendle, M., Bowman, M.E., Noel, J.P.,
714 Gruebele, M. and Kelly, J.W., 2006. Structure–function–folding relationship in a WW
715 domain. *Proceedings of the National Academy of Sciences*, *103*(28), pp.10648-10653.
716 17. Ingham, R.J., Colwill, K., Howard, C., Dettwiler, S., Lim, C.S., Yu, J., Hersi, K.,
717 Raaijmakers, J., Gish, G., Mbamalu, G. and Taylor, L., 2005. WW domains provide a
718 platform for the assembly of multiprotein networks. *Molecular and cellular biology*,
719 *25*(16), pp.7092-7106.
720 18. Sudol, M., 2010. Newcomers to the WW domain–mediated network of the Hippo tumor
721 suppressor pathway. *Genes & cancer*, *1*(11), pp.1115-1118.
722 19. Salah, Z., Alian, A. and Aqeilan, R.I., 2012. WW domain-containing proteins:
723 retrospectives and the future. *Front Biosci*, *17*, pp.331-348.

724 20. Lin, Z., Yang, Z., Xie, R., Ji, Z., Guan, K. and Zhang, M., 2019. Decoding WW domain
725 tandem-mediated target recognitions in tissue growth and cell polarity. *Elife*, *8*,
726 p.e49439.
727 21. Ilsley, J.L., Sudol, M. and Winder, S.J., 2002. The WW domain: linking cell signalling
728 to the membrane cytoskeleton. *Cellular signalling*, *14*(3), pp.183-189.
729 22. Pucheta-Martinez, E., D'Amelio, N., Lelli, M., Martinez-Torrecuadrada, J.L., Sudol, M.,
730 Saladino, G. and Gervasio, F.L., 2016. Changes in the folding landscape of the WW
731 domain provide a molecular mechanism for an inherited genetic syndrome. *Scientific*
732 *reports*, *6*(1), pp.1-8.
733 23. Chang, N.S., Lin, R., Sze, C.I. and Aqeilan, R.I., 2019. WW Domain Proteins in
734 Signaling, Cancer Growth, Neural Diseases, and Metabolic Disorders. *Frontiers in*
735 *oncology*, *9*, p.719.
736 24. Sudol, M., McDonald, C.B. and Farooq, A., 2012. Molecular insights into the WW
737 domain of the Golabi-Ito-Hall syndrome protein PQBP1. *FEBS letters*, *586*(17),
738 pp.2795-2799.
739 25. Kunkle, B.W., Grenier-Boley, B., Sims, R., Bis, J.C., Damotte, V., Naj, A.C., Boland,
740 A., Vronskaya, M., Van Der Lee, S.J., Amlie-Wolf, A. and Bellenguez, C., 2019.
741 Genetic meta-analysis of diagnosed Alzheimer's disease identifies new risk loci and
742 implicates Aβ, tau, immunity and lipid processing. *Nature genetics*, *51*(3), pp.414-430.
743 26. Salah, Z. and Aqeilan, R.I., 2011. WW domain interactions regulate the Hippo tumor
744 suppressor pathway. *Cell death & disease*, *2*(6), pp.e172-e172.
745 27. Lee, H.L., Cheng, H.L., Liu, Y.F., Chou, M.C., Yang, S.F. and Chou, Y.E., 2017.
746 Functional genetic variant of WW domain-containing oxidoreductase (WWOX) gene is
747 associated with hepatocellular carcinoma risk. *PLoS One*, *12*(4), p.e0176141.
748 28. Hung, S.C., Chou, Y.E., Li, J.R., Chen, C.S., Lin, C.Y., Chang, L.W., Chiu, K.Y., Cheng,
749 C.L., Ou, Y.C., Wang, S.S. and Yang, S.F., 2020, February. Functional genetic variant
750 of ww domain containing oxidoreductase gene associated with urothelial cell

751 carcinoma clinicopathologic characteristics and long-term survival. In *Urologic*
752 *Oncology: Seminars and Original Investigations* (Vol. 38, No. 2, pp. 41-e1). Elsevier.
753 29. Xie, P., Tian, C., An, L., Nie, J., Lu, K., Xing, G., Zhang, L. and He, F., 2008. Histone
754 methyltransferase protein SETD2 interacts with p53 and selectively regulates its
755 downstream genes. *Cellular signalling*, *20*(9), pp.1671-1678.
756 30. Seervai, R.N., Jangid, R.K., Karki, M., Tripathi, D.N., Jung, S.Y., Kearns, S.E., Verhey,
757 K.J., Cianfrocco, M.A., Millis, B.A., Tyska, M.J. and Mason, F.M., 2020. The Huntingtin-
758 interacting protein SETD2/HYPB is an actin lysine methyltransferase. *Science*
759 *advances*, *6*(40), p.eabb7854.
760 31. Cisbani, G. and Cicchetti, F., 2012. An in vitro perspective on the molecular
761 mechanisms underlying mutant huntingtin protein toxicity. *Cell death & disease*, *3*(8),
762 pp.e382-e382.
763 32. Yount, J.S., Kraus, T.A., Horvath, C.M., Moran, T.M. and López, C.B., 2006. A novel
764 role for viral-defective interfering particles in enhancing dendritic cell maturation. *The*
765 *Journal of Immunology*, *177*(7), pp.4503-4513.
766 33. Skene, P.J., Henikoff, J.G. and Henikoff, S., 2018. Targeted in situ genome-wide
767 profiling with high efficiency for low cell numbers. *Nature protocols*, *13*(5), p.1006.
768 34. Schneider, C.A., Rasband, W.S. and Eliceiri, K.W., 2012. NIH Image to ImageJ: 25
769 years of image analysis. *Nature methods*, *9*(7), pp.671-675.
770 35. Laliotis, Georgios I; Chavdoula, Evangelia; Anastas, Vollter; Singh, Satishkumar;
771 Kenney, Adam D. ; Achaya, Samir; Yount, Jacob S.; Sehgal, Lalit; Tsichlis, Philip N.
772 (2021), “Overexpression of the SETD2 WW domain inhibits the phosphor-
773 IWS1/SETD2 interaction and the oncogenic AKT/IWS1 RNA splicing program.”,
774 Mendeley Data, V1, doi: 10.17632/d5kv2dyhc4.1
775
776
777

778 **Figure Legends**

779

780 **Figure 1. The interaction between SETD2 and phosphorylated IWS1 is mediated by the**
781 **WW domain of SETD2.**

782 **A.** Graphical representation of the SETD2 deletion mutants (1-8) used in this study. AWS
783 : Associated with SET, SET : Su(var)3–9, Enhancer-of-zeste, Trithorax, PS : post-SET,
784 LCR : Low Charge Region, WW, SRI : Set2 Rpb1-interacting.

785 **B. and C.** NCI-H522 and NCI-H1299 cells were transiently transfected with the SETD2
786 deletion mutants. Anti-HA, anti-IgG rabbit isotype control immunoprecipitates and input
787 lysates were probed with the indicated antibodies.

788 **Figure 2. SETD2-WW domain binds phosphorylated IWS1 and disrupts the endogenous**
789 **IWS1-SETD2 interaction.**

790 **A.** NCI-H522, NCI-H1299 (upper panel), A549 and NCI-H1975 (lower panel), were
791 transduced with the indicated constructs. Anti-V5, anti-IgG rabbit isotype control
792 immunoprecipitates and input lysates were probed with the indicated antibodies.

793 **B.** NCI-H522, NCI-H1299 (upper panel), A549 and NCI-H1975 (lower panel), were
794 transduced with the indicated constructs. Anti-Flag, anti-IgG rabbit isotype control
795 immunoprecipitates and input lysates were probed with the indicated antibodies.

796 **C.** NCI-H522, NCI-H1299 (upper panel), A549 and NCI-H1975 (lower panel), were
797 transduced with the indicated constructs. Anti-IWS1, anti-IgG rabbit isotype control
798 immunoprecipitates and input lysates were probed with the indicated antibodies.

799

800

801

802 **Figure 3. The overexpression of SETD2 WW domain inhibits the downstream IWS1**
803 **phosphorylation-dependent RNA splicing program.**

804 **A.** *Overexpression of the SETD2 WW domain inhibits the IWS1-dependent RNA splicing*
805 *program.* (Upper lanes) NCI-H522, NCI-H1299, A549 and NCI-H1975, were
806 transduced with the indicated constructs and their lysates probed with the indicated
807 antibodies. (Lower lanes) RT-PCR examining the exon usage of the known IWS1 RNA
808 splicing targets *U2AF2* (exon 2), *SLC12A2* (exon 21), *IFT88* (exon 8), *STXBP1* (exon
809 18) and *C1qTNF6* (exon 3). *GAPDH* was used as control.

810 **B.** Quantitative RT-PCR showing the E2/E3 and IIIb/IIIc ratio in the *U2AF2* (upper panel)
811 and *FGFR2* (lower panel) mRNA transcripts in shControl, shIWS1 and pLx304 SETD2
812 WW-V5 NCI-H522, NCI-H1299, A549 and NCI-H1975 cells. Bars show the E2/E3 or
813 IIIb/IIIc ratio (mean ± SD) in all the cell lines, relative to the shControl.

814 **C. and D.** ChIC assays of SETD2 and H3K36me3 abundance in the indicated regions of
815 *U2AF2*, *FGFR2* and *GAPDH* genes, in the same cells as in 3A. Bars show the mean
816 fold enrichment (anti-SETD2 IP and anti-H3K36me3 IP vs anti-IgG IP) ±SD. Data were
817 normalized relative to the input (2%). All assays were done in triplicate, on three
818 biological replicates. n.s : non-significant *p<0.05, **p<0.01, ***p<0.001, ****p<0.0001.
819 (one-side unpaired t-test)

820 **Figure 4. The overexpression of SETD2 WW domain inhibits the downstream IWS1**
821 **phosphorylation-dependent pathways.**

822 **A.** The indicated cells as in 3A, were probed with the indicated antibodies of the
823 Sororin/ERK phosphorylation pathway.

824 **B.** Western blots of lysates of the same cells, were probed with the indicated antibodies.
825 For type I IFN induction SeV-GFP infection was performed (NCI-H522 : MOI=0.5 for
826 16h, NCI-H1299 : MOI of 0.25 for 24h of SeV-GFP virus).

827 **Figure 5. The overexpression of SETD2 WW domain inhibits cell proliferation, cell cycle**
828 **progression and cell transformation in lung adenocarcinoma.**

829 **A.** Growth curves of the indicated NCI-H522, NCI-H1299, A549 and NCI-H1975 cells in
830 media supplemented with 10% FBS. Cell proliferation was measured every 6 hours in
831 three independent cultures and expressed as confluence mean percentages±SD. For
832 simplicity, 12h points are shown. *P* values were calculated for the endpoint
833 measurements, using the one-side unpaired t-test. *p<0.05, **p<0.01, ***p<0.001,
834 ****p<0.0001

835 **B.** Cell cycle profiles of the indicated propidium iodide (PI)-stained cell lines. Figure shows
836 one representative, out of three biological replicates. Numbers in red show the mean
837 percentage of cells in different phases of the cell cycle and the *P* value using unpaired
838 one-sided t test between shCon vs shIWS1 or vs pLx304 WW.

839 **C.** Growth curves of the indicated NCI-H522, NCI-H1299, A549 and NCI-H1975 cells in
840 media supplemented with 10% FBS. Live-cell numbers (mean ±SD) were measured
841 with the alamarBlue™ Cell Viability Reagent in three independent cultures for each
842 cell type. The expression of V5-U2AF65 isoforms is shown in Supplementary Figure
843 1A.

844 **D.** (Upper panel) HBEC hTERT cells transduced with the indicated constructs, were
845 subjected to cell transformation assay for 7 days. At that time point the cells were
846 imaged. Scale bar in the right corner of each image. (Lower left panel) Validation of
847 the cells used in the transformation assay by probing wetern blot lysates with the
848 indicated antibodies. (Lower right panel) After imaging, the cells were incubated for 4
849 hours in WST solution as described in the Cell Transformation Assay Kit (Abcam). Bars
850 show the number of transformed cells as measured in absorbance 450nm ±SD. All
851 assays in this figure were done in triplicate, on three biological replicates. n.s : non-
852 significant *p<0.05, **p<0.01, ***p<0.001, ****p<0.0001. (one-side unpaired t-test).

853 **Figure 6. The overexpression of SETD2 WW domain inhibits tumor growth and the IWS1**
854 **phosphorylation pathway *in vivo*.**

855 **A.** *Summary of the experimental design.* Schematic of the mouse groups used in this
856 study (Upper panel), along with their downstream applications (Lower panel).
857 Specifically, 2 mice from each group were used for IP experiments, while 5 were used
858 for RNA and protein extraction. The NCI-H1299 shIWS1-derived tumors of group 1
859 were stored for future use.

860 **B.** NSG mice were injected subcutaneously with shControl or shIWS1 (group 1) or
861 shIWS1 or pLx304 SETD2 WW (group 2) $2x10^6$ NCI-H1299 cells. (N=7 mice/group).
862 Images of the induced tumors, harvested at 4 weeks from the time of inoculation.
863 Scatter plots showing the tumor weight and volume of the tumors. The horizontal lines
864 indicate mean tumor weight or volume. Statistical analyses were done using one-sided
865 paired t-test.

866 ***C.*** *The overexpression of the SETD2 WW domain inhibits the IWS1/SETD2 interaction in*
867 *vivo.* The indicated tumors from the xenografts model in 6a were harvested and
868 subjected to IP experiments. The anti-IWS1 IP and anti-IgG immunoprecipitation and
869 input lysates were probed with the indicated antibodies.

870 **D.** *The overexpression of the SETD2 WW domain inhibits the IWS1-dependent pathways*
871 *in vivo.* Cell lysates derived from the indicated mouse xenograft tumors, were probed
872 with the indicated antibodies. RT-PCR of *U2AF2* E2, *SLC12A2* E21, *IFT88* E8,
873 *C1qTNF6* E3, *STXBP1* E18 from the same tumors.

874 **E.** Formalin-fixed, paraffin-embedded tumor samples from the experiment in Figure 6a
875 were stained with the indicated antibodies. Secondary antibody was HRP-labelled.
876 Scale in the right lower corner of each image.

877 **F.** Scatter plots showing IHC signal of the indicated marker relative to the section area in
878 the mouse xenograft tumors. The horizontal line shows the mean signal in the indicated

879 groups of xenografts. Statistical analyses were performed, using the one-sided paired
880 t-test.

881 **Figure 7. Graphical abstract of the findings.**

882 The overexpression of the SETD2 WW domain antagonizes the interaction of phosphorylated
883 IWS1 with SETD2 and its recruitment in IWS1-dependent RNA splicing targets. This affects
884 the H3K36me3 distribution and subsequent oncogenic AKT/IWS1 RNA splicing program,
885 inhibiting tumor growth. This interaction and chemical affinity of the WW domain can be used
886 as a drug screening platform for the IWS1/SETD2 complex in lung adenocarcinoma.
887

Figure 1

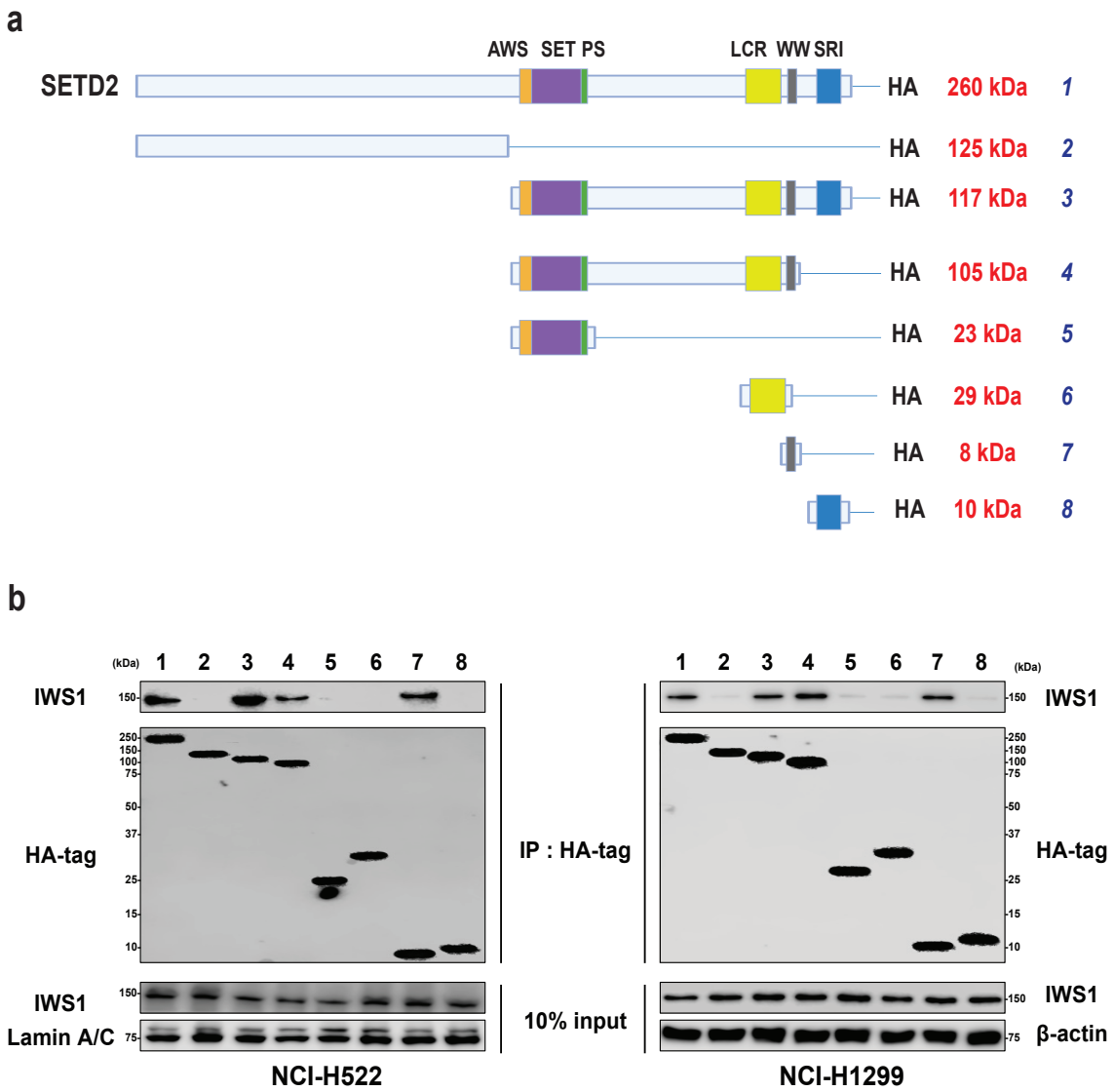
a
AWS SET PS
LCR WW SRI
SETD2
HA 260 kDa 1
HA 125 kDa 2
HA 117 kDa 3
HA 105 kDa 4
HA 23 kDa 5
HA 29 kDa 6
HA 8 kDa 7
HA 10 kDa 8
b
(kDa) 1 2 3 4 5 6 7 8
IWS1
HA-tag
IWS1
Lamin A/C
IP : HA-tag
10% input
IWS1
HA-tag
IWS1
β-actin
NCI-H522
NCI-H1299

Figure 2

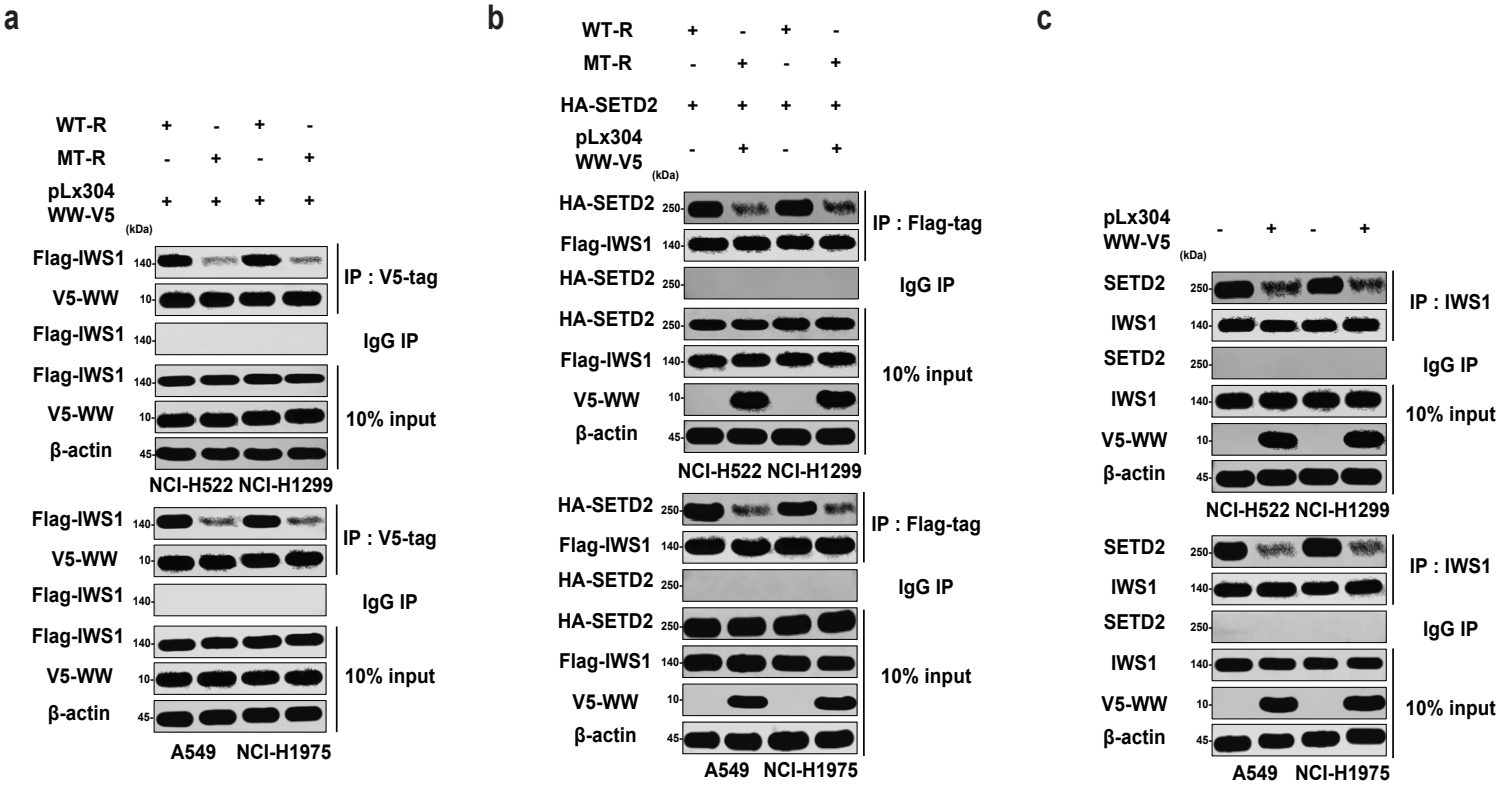
a
WT-R + - + -
MT-R - + - +
pLx304 WW-V5 + + + +
(kDa)
Flag-IWS1 140-
V5-WW 10-
IP : V5-tag
Flag-IWS1 140-
IgG IP
Flag-IWS1 140-
V5-WW 10-
β-actin 45-
10% input
NCI-H522 NCI-H1299
Flag-IWS1 140-
V5-WW 10-
IP : V5-tag
Flag-IWS1 140-
IgG IP
Flag-IWS1 140-
V5-WW 10-
β-actin 45-
10% input
A549 NCI-H1975
b
WT-R + - + -
MT-R - + - +
HA-SETD2 + + + +
pLx304 WW-V5 - + - +
(kDa)
HA-SETD2 250-
Flag-IWS1 140-
IP : Flag-tag
HA-SETD2 250-
IgG IP
HA-SETD2 250-
Flag-IWS1 140-
V5-WW 10-
β-actin 45-
10% input
NCI-H522 NCI-H1299
HA-SETD2 250-
Flag-IWS1 140-
IP : Flag-tag
HA-SETD2 250-
IgG IP
HA-SETD2 250-
Flag-IWS1 140-
V5-WW 10-
β-actin 45-
10% input
A549 NCI-H1975
c
pLx304 WW-V5 - + - +
(kDa)
SETD2 250-
IWS1 140-
IP : IWS1
SETD2 250-
IgG IP
IWS1 140-
V5-WW 10-
β-actin 45-
10% input
NCI-H522 NCI-H1299
SETD2 250-
IWS1 140-
IP : IWS1
SETD2 250-
IgG IP
IWS1 140-
V5-WW 10-
β-actin 45-
10% input
A549 NCI-H1975

Figure 3

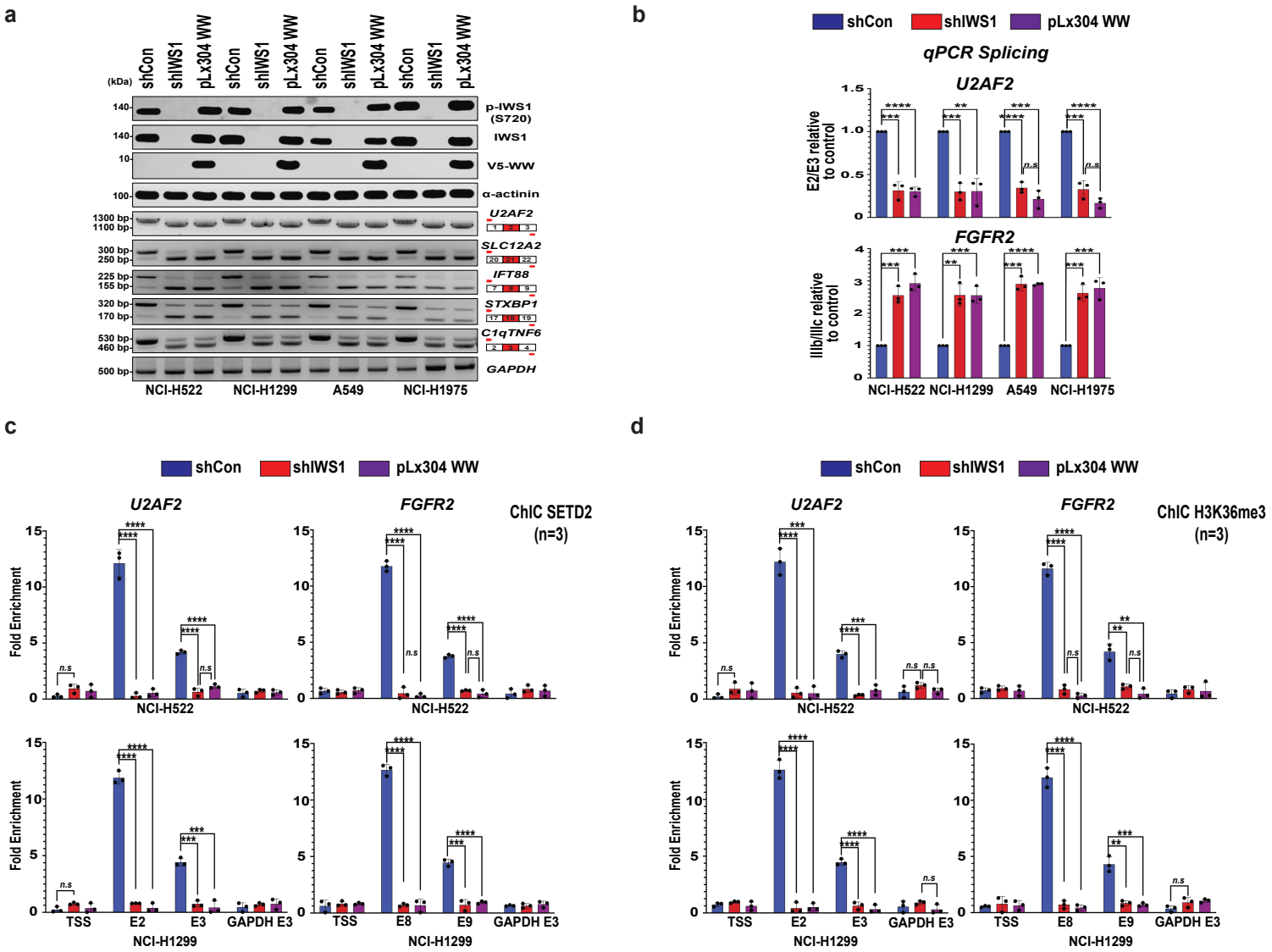
a
shCon
shIWS1
pLx304 WW
(kDa)
140
p-IWS1 (S720)
IWS1
10
V5-WW
100
α-actinin
1300 bp
1100 bp
U2AF2
300 bp
250 bp
SLC12A2
225 bp
155 bp
IFT88
320 bp
170 bp
STXBP1
530 bp
460 bp
C1qTNF6
500 bp
GAPDH
NCI-H522
NCI-H1299
A549
NCI-H1975
b
qPCR Splicing
U2AF2
E2/E3 relative to control
FGFR2
IIIb/IIIc relative to control
c
ChIC SETD2 (n=3)
Fold Enrichment
TSS
E2
E3
GAPDH E3
E8
E9
d
ChIC H3K36me3 (n=3)

Figure 4

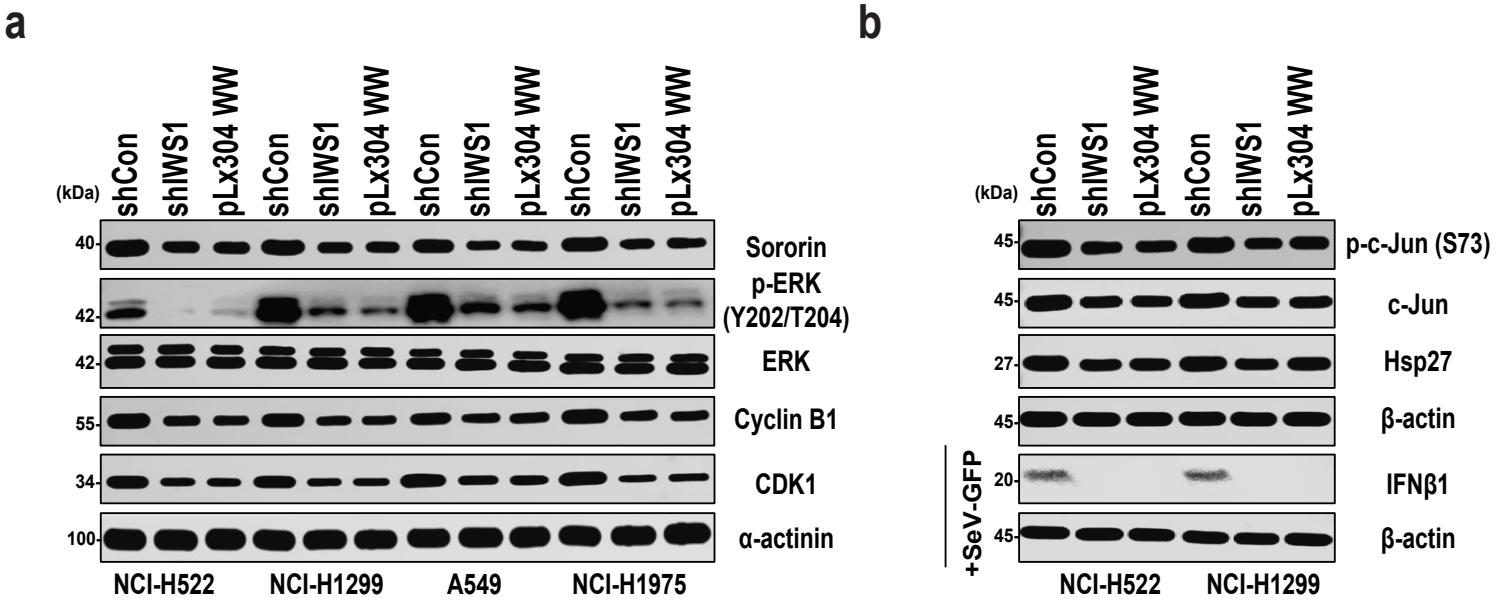
a
(kDa)
shCon
shIWS1
pLx304 WW
shCon
shIWS1
pLx304 WW
shCon
shIWS1
pLx304 WW
shCon
shIWS1
pLx304 WW
40-
42-
42-
55-
34-
100-
Sororin
p-ERK
(Y202/T204)
ERK
Cyclin B1
CDK1
α-actinin
NCI-H522
NCI-H1299
A549
NCI-H1975
b
(kDa)
shCon
shIWS1
pLx304 WW
shCon
shIWS1
pLx304 WW
45-
45-
27-
45-
20-
45-
p-c-Jun (S73)
c-Jun
Hsp27
β-actin
IFNβ1
β-actin
+SeV-GFP
NCI-H522
NCI-H1299

Figure 5

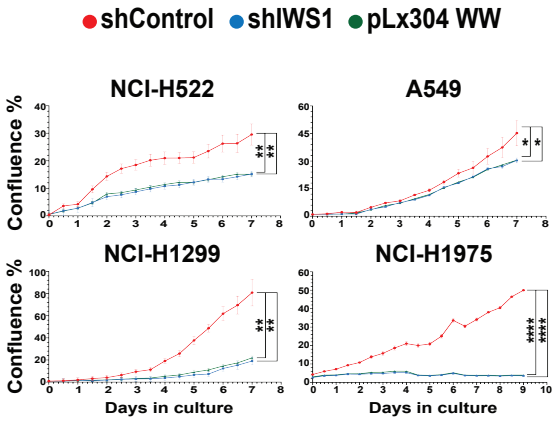
a
shControl
shIWS1
pLx304 WW
NCI-H522
A549
NCI-H1299
NCI-H1975
Confluence %
Days in culture

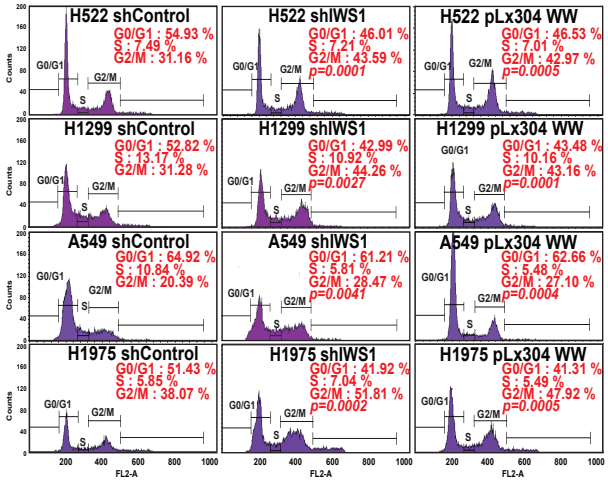
b
H522 shControl
G0/G1 : 54.93 %
S : 7.49 %
G2/M : 31.16 %
H522 shIWS1
G0/G1 : 46.01 %
S : 7.21 %
G2/M : 43.59 %
p=0.0001
H522 pLx304 WW
G0/G1 : 46.53 %
S : 7.01 %
G2/M : 42.97 %
p=0.0005
H1299 shControl
G0/G1 : 52.82 %
S : 13.17 %
G2/M : 31.28 %
H1299 shIWS1
G0/G1 : 42.99 %
S : 10.92 %
G2/M : 44.26 %
p=0.0027
H1299 pLx304 WW
G0/G1 : 43.48 %
S : 10.16 %
G2/M : 43.16 %
p=0.0001
A549 shControl
G0/G1 : 64.92 %
S : 10.84 %
G2/M : 20.39 %
A549 shIWS1
G0/G1 : 61.21 %
S : 5.81 %
G2/M : 28.47 %
p=0.0041
A549 pLx304 WW
G0/G1 : 62.66 %
S : 5.48 %
G2/M : 27.10 %
p=0.0004
H1975 shControl
G0/G1 : 51.43 %
S : 5.85 %
G2/M : 38.07 %
H1975 shIWS1
G0/G1 : 41.92 %
S : 7.04 %
G2/M : 51.81 %
p=0.0002
H1975 pLx304 WW
G0/G1 : 41.31 %
S : 5.49 %
G2/M : 47.92 %
p=0.0005
Counts
FL2-A

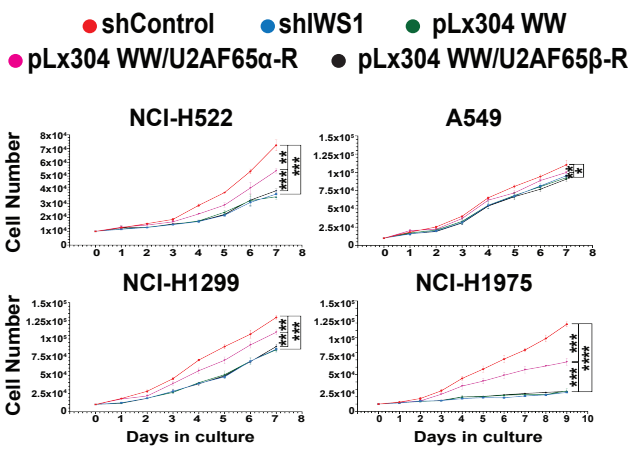
c
shControl
shIWS1
pLx304 WW
pLx304 WW/U2AF65α-R
pLx304 WW/U2AF65β-R
NCI-H522
A549
NCI-H1299
NCI-H1975
Cell Number
Days in culture

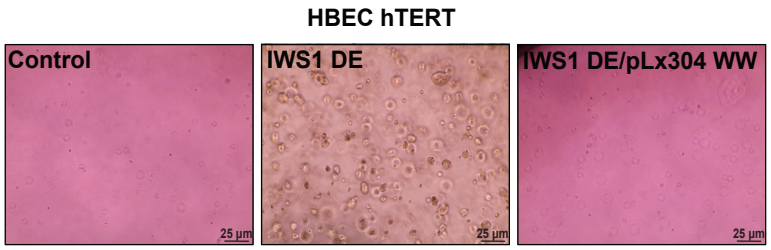
d
HBEC hTERT
Control
IWS1 DE
IWS1 DE/pLx304 WW
25 μm

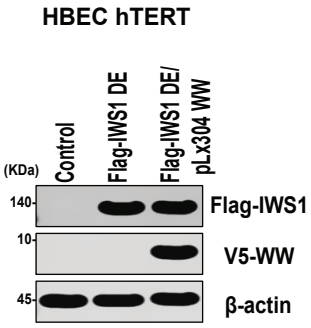
HBEC hTERT
(KDa)
Control
Flag-IWS1 DE
Flag-IWS1 DE/ pLx304 WW
140
10
45
Flag-IWS1
V5-WW
β-actin

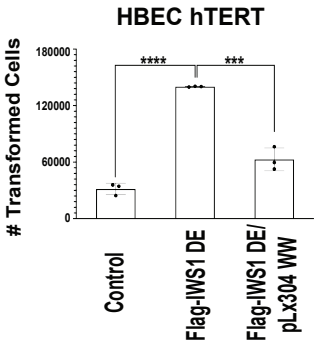
HBEC hTERT
Transformed Cells
Control
Flag-IWS1 DE
Flag-IWS1 DE/ pLx304 WW

Figure 6

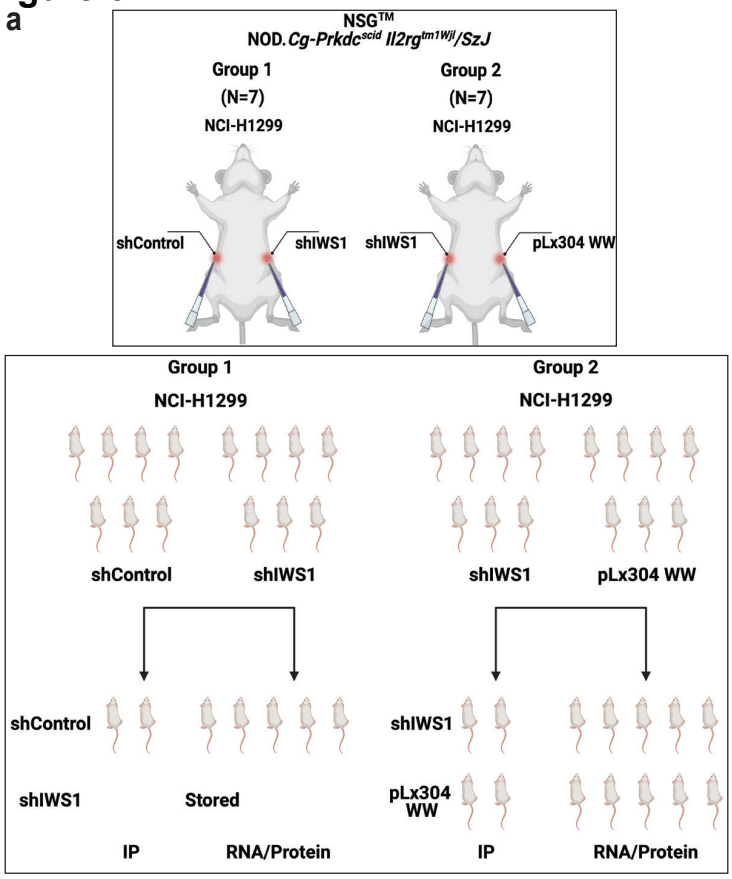
a
NSG™
NOD.Cg-Prkdc scid Il2rg tm1Wjl/SzJ
Group 1
(N=7)
NCI-H1299
Group 2
(N=7)
NCI-H1299
shControl
shIWS1
shIWS1
pLx304 WW
Group 1
NCI-H1299
Group 2
NCI-H1299
shControl
shIWS1
shIWS1
pLx304 WW
shControl
shIWS1
Stored
IP
RNA/Protein
shIWS1
pLx304 WW
IP
RNA/Protein

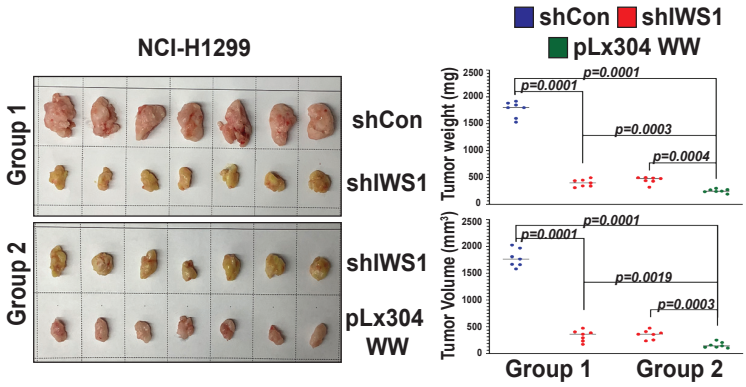
b
NCI-H1299
shCon
shIWS1
pLx304 WW
Group 1
Group 2
shCon
shIWS1
shIWS1
pLx304 WW
Tumor weight (mg)
Tumor Volume (mm³)
p=0.0001
p=0.0003
p=0.0004
p=0.0001
p=0.0001
p=0.0019
p=0.0003
Group 1
Group 2

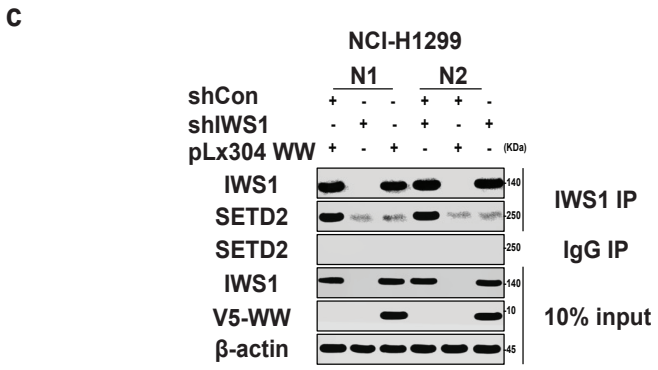
c
NCI-H1299
N1
N2
shCon
shIWS1
pLx304 WW
(KDa)
IWS1
SETD2
SETD2
IWS1
V5-WW
β-actin
IWS1 IP
IgG IP
10% input

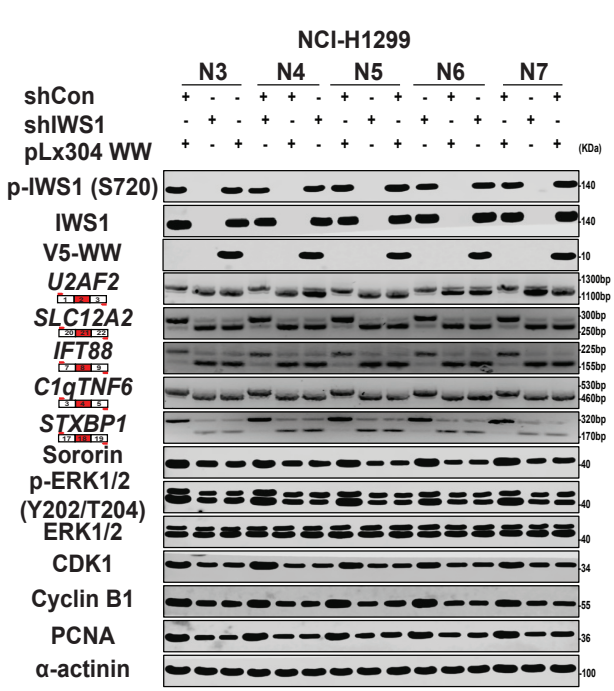
d
NCI-H1299
N3
N4
N5
N6
N7
shCon
shIWS1
pLx304 WW
(KDa)
p-IWS1 (S720)
IWS1
V5-WW
U2AF2
SLC12A2
IFT88
C1qTNF6
STXBP1
Sororin
p-ERK1/2 (Y202/T204)
ERK1/2
CDK1
Cyclin B1
PCNA
α-actinin

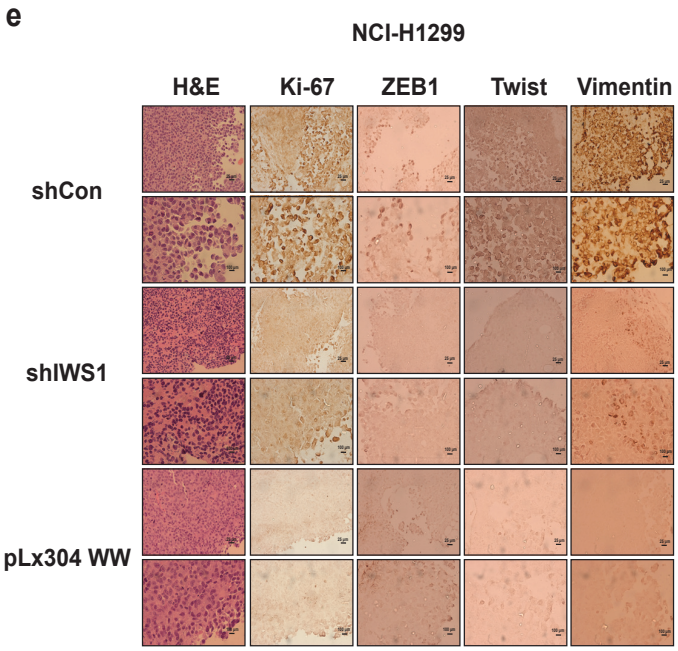
e
NCI-H1299
H&E
Ki-67
ZEB1
Twist
Vimentin
shCon
shIWS1
pLx304 WW

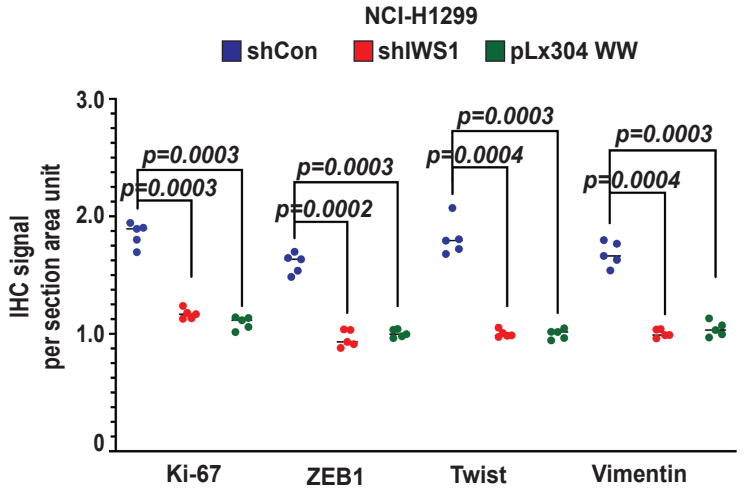
f
NCI-H1299
shCon
shIWS1
pLx304 WW
IHC signal per section area unit
p=0.0003
p=0.0003
p=0.0003
p=0.0002
p=0.0003
p=0.0004
p=0.0003
p=0.0004
Ki-67
ZEB1
Twist
Vimentin

Figure 7

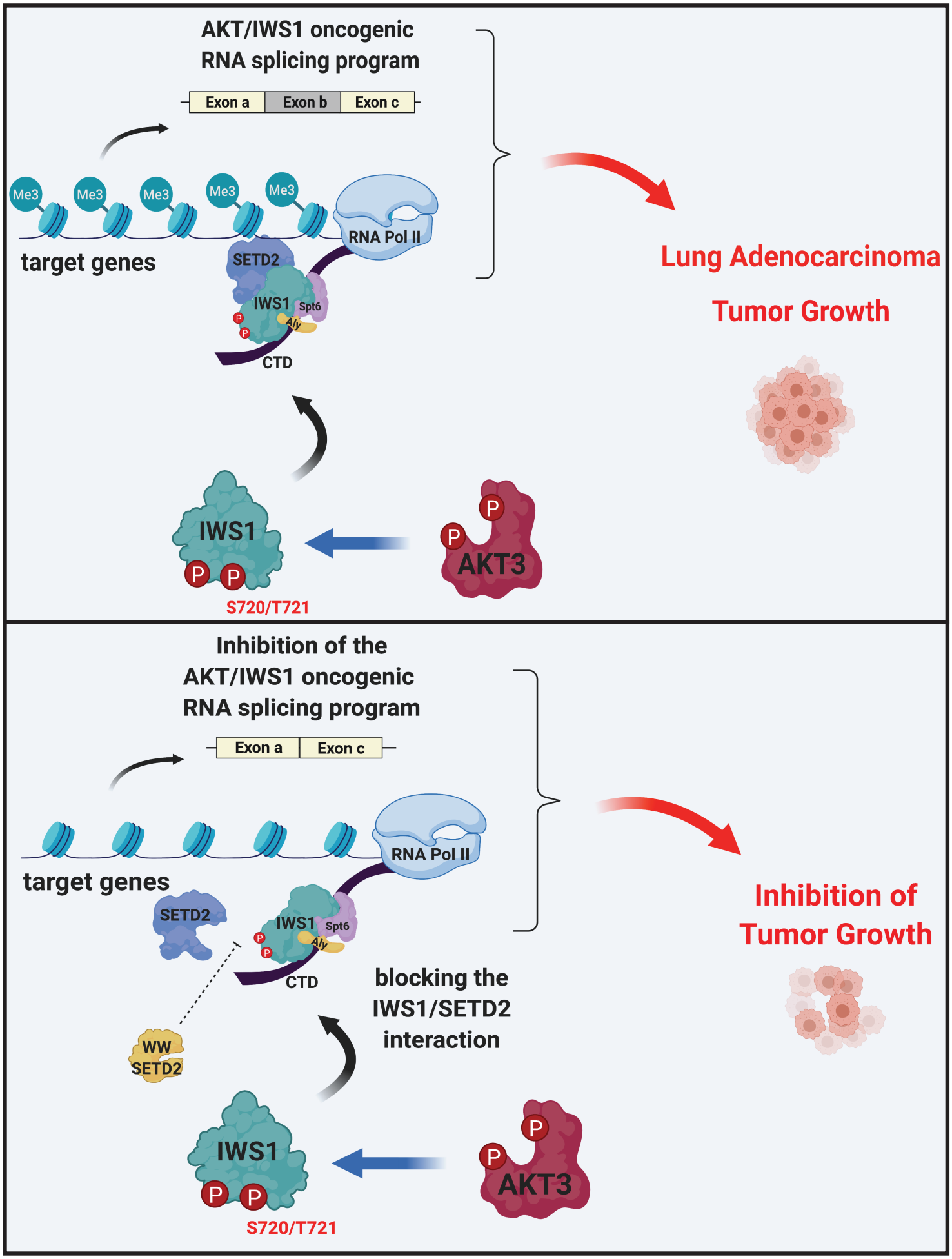
AKT/IWS1 oncogenic
RNA splicing program
Exon a
Exon b
Exon c
Me3
target genes
SETD2
RNA Pol II
IWS1
Spt6
Aly
CTD
Lung Adenocarcinoma
Tumor Growth
IWS1
S720/T721
AKT3
Inhibition of the
AKT/IWS1 oncogenic
RNA splicing program
Exon a
Exon c
target genes
SETD2
RNA Pol II
IWS1
Spt6
Aly
CTD
WW
SETD2
blocking the
IWS1/SETD2
interaction
Inhibition of
Tumor Growth
IWS1
S720/T721
AKT3